NTNU

Norwegian University of
Science and Technology

Automatic Start-up and Control of Artificially Lifted Wells

Rasmus Rønning

Master of Science in Engineering Cybernetics
Submission date: September 2011
Supervisor: Ole Morten Aamo, ITK
Co-supervisor: Alexey Pavlov, Statoil

Norwegian University of Science and Technology
Department of Engineering Cybernetics

Summary

Artificial lift in oil wells using a downhole pump has received much attention the last decades and is established as a reliable and efficient lifting method. In particular, artificial lift using an *electric submersible pump (EPS)* has proven to be an important alternative in deep wells with high production rate requirements.

This thesis investigate the problem of controlling the ESP intake pressure under rigid ESP operational constraints and input requirements, using the ESP frequency and choke position as control inputs.

A mathematical model of a system containing ESP lifted wells is created and a control strategy that fulfil the control requirements is proposed. The model is an extension of the ESP model developed by Amundsen et al. [2010] and contain four ESP lifted wells. Mathematical proof of open-loop stability is derived based on analysis of a linearized well model. Also, closed-loop stability for the linearized model is proved based on frequency analysis.

The proposed control strategy is tested on the model in a range of different case study. The control system display a capability of minimizing the control error while keeping the ESP operated within the given constraints, with an optimal combination of control inputs. Simulation results indicate that the proposed control strategy is capable of handling a step-change in ESP intake pressure, ESP tripping, and ESP and booster-pump start-up/shut-down.

Preface

This report is submitted as my master thesis in the Master of Science program in Engineering Cybernetics at the Norwegian University of Science and Technology.

This thesis mark the end of a five year period of study which has been both challenging and rewarding. It is with a sense of pride and content, that I now perform the finishing touch on my thesis.

I would like to thank my supervisor Professor Ole Morten Aamo for helpful discussions throughout the semester and non the least, Dr. Alexey Pavlov for providing important support and expert knowledge. You're help have been greatly appreciated. I would also like to thank Torunn, who has been my partner throughout my years of study, for her love and support.

Stavanger, September 18th 2011
Rasmus Rønning

Contents

Nomenclature

β	Bulk modulus
μ	Dynamic viscosity
ν	Kinematic viscosity
ρ	Density
A	Cross-section area
d	Inner pipe diameter
F	Friction force
g	Gravitational acceleration
H	Head unit
p	Pressure
q	Volumetric flow
v	Fluid velocity
w	Mass flow

Chapter 1

Introduction

1.1 Background

Production of crude oil is accomplished by drilling an oil well from the earth's surface, down into a rock formation that contain a pressurized reservoir of hydrocarbons and natural gas. If the reservoir pressure is sufficient to overcome the sum of pressure losses occurring along the flow path, natural flow from the reservoir to the surface occurs. As the reservoar is depleted the pressure gradually decrease and at some point in time, this may effect the natural flow through the well.

A technique that may be applied to counteract reduced flow through the well is so-called *artificial lift*, where the general idea is to reduce pressure loss occurring along the flow path from the reservoir to the surface. By reducing pressure losses along the flow path, a sufficient pressure gradient is uphold to maintain a desired flow rate. It is customary to classify artificial lift methods into two main categories; gas lift and pumping.

Gas lift involve injection of high-pressure natural gas in the well stream at some downhole point. Injection of gas at a steady rate (continuous flow gas lift) or periodically (intermittent gas lift) into the flow lead to a reduction in flow mixture density and consequently, a reduction in pressure loss due to reduced flow resistance.

Pumping involve use of a downhole pump to overcome pressure losses along the flow path by increasing pressure in the well. *Electric submersible pumping (ESP)* is a variant of this pumping technique that utilize a submerged electrical motor to drive a multistage centrifugal pump. A principal sketch is illustrated in figure 1.1.

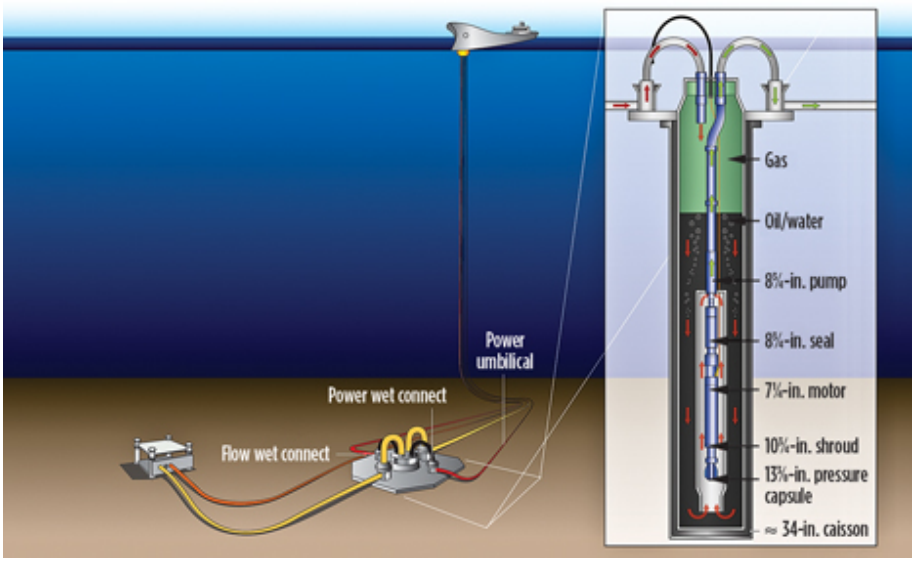

Figure 1.1: A principal sketch of a downhole ESP unit. The figure outlines a Baker Hughes Centerlift ESP system used in subsea separation. Courtesy of Baker Hughes, www.maritimeprofessional.com.

ESP units are capable of lifting much greater liquid rates than most of the other types of artificial lift and are often used in high rate on- and offshore applications. Some of the general advantages of using ESP is that it can produce high liquid volumes in an energy efficient manner, it requires a low grade of maintenance and it has low topside space requirements.

One of the more important disadvantages with ESP is high costs related to maintenance and repair. Since the ESP unit is located downhole the tubing string must be removed in order to access the ESP and this requires use of heavy workover units. There is also a substantial down-time associated with the operation of removing and replacing an ESP, where production from the well halts. Thus, it is important that the lifetime of the ESP is as long as possible and that required maintenance and repair is kept at a minimum.

Expected lifetime and maintenance frequency of an ESP unit is correlated with how the ESP is operated. Takacs [2009] states that axial forces occurring in the pump is a decisive factor when it comes to wear and tear of the ESP, and suggest that an ESP should be operated within a spesific range

of operation about the best efficiency point (BEP) which is determined by some optimization criteria. Outside this range of operation, static and dynamic axial forces occurring in the pump might lead to certain phenomena known as downthrust and upthrust.

Downthrust is the downward force that the impeller and shaft assembly experience when the pump is in operation. Most ESP units are designed to operate under a continuous downthrust condition, but too much downthrust can create problems. Downthrust problems occur when the pump is running with a very low liquid rate, resulting in higher discharge pressure and higher downthrust load.

Upthrust is a condition where there is an upward force on the shaft and impeller assembly. This condition is caused when the pump is pumping more liquid than it was designed to produce. Upthrust is potentially more dangerous than downthrust due to the low load-bearing area in the pump.

The safe range of operation impose severe restrictions on ESP applications which should be met at all times. Operation within the safe range can be achieved by manual or automatic control of the ESP. Automatic control offer severeral benefits over manual control such as extended range of application and less operator demands.

1.2 Scope

The objective in this thesis is to investigate the possibility of designing an automatic control system that ensure ESP operation within the safe range of operation. In this context the safe range of operation is given by an *operational envelope*, which represent a set of constraints in flow rate through the ESP and differential pressure exerted by the ESP.

The intension is to develop a control system that is able to handle a set of different situations relevant to actual ESP operation by using a limited set of control inputs. In addition, the control system should be able to handle given restrictions on the use of the different control inputs.

Behavior of the control system is to be tested and assessed on an extended model deduced from the ESP model developed by Statoil.

1.3 Thesis outline

This thesis starts with a preliminary chapter where common mathematical definitions and abbreviations are presented. Then, mathematical models for an ESP lifted well and associated components are presented in Chapter 3.

Chapter 4 deals with the control aspect in this thesis. Here, the ESP operational constraints is presented and a control strategy that enable both pressure control and envelope handling is proposed. In the following, open- and closed-loop stability analysis is performed in Chapter 5.

Then, a set of case study is performed in Chapter 6 where the proposed control strategy is tested on the model in a simulation environment. Finally, conclusions are presented in Chapter 7, and future work is proposed.

Chapter 2

Preliminaries

2.1 Mathematical conventions

Vectors and matrices are written in boldface, while scalars are not. Vector and matrix transposed and inverse are denoted $\mathbf{x}^\top$and $\mathbf{x}^{-1}$, respectively. The domain $\mathbb{R}^d$ of a variable are defined as an Euclidian d-dimensional space. Time derivative of $\mathbf{x}(t)$ are denoted $\dot{\mathbf{x}}$, $\ddot{\mathbf{x}}$, $\cdots$, $\mathbf{x}^{(i)}$, while derivatives with respect to another variable are denoted $\frac{\delta \mathbf{x}}{\delta x_i}$, $\frac{\delta^2 \mathbf{x}}{\delta x_i^2}$, $\cdots$ $\frac{\delta^{(i)} \mathbf{x}}{\delta x_i^{(i)}}$. Vector norm $|\mathbf{x}|$ is defined as the Euclidian norm $\sqrt{\mathbf{x}^\top \mathbf{x}}$, and a matrix norm $||\mathbf{x}||$ is defined as the Forbenius norm $||\mathbf{x}|| = \left(\sum_{i,j} |x_{ij}|^2 \right)^{1/2}$. In the scalar case, $|x|$ denotes the absolute value of $x \in \mathbb{R}^+$.

2.2 Abbreviations

Several uncommon abbreviations are used throughout the report. These abbreviations are presented in the succeeding table

ESP	Electric submersible pump
BP	Booster-pump
VFD	Variable frequency drive
VFG	Variable frequency generator
WC	Water cut
BEP	Best efficiency point

Chapter 3

Mathematical Modeling

The mathematical model presented in this chapter is an extension of the ESP model derived by Amundsen et al. [2010]. A general description of the overall system is provided in section 3.1 and a model for the different parts of the system is deduced in section 3.2 to 3.6. The complete simulation model is presented in section 3.7.

3.1 System description

The mathematical model derived in this chapter depict an oil producing installation containing ESP lifted wells. The system contain a set of four ESP lifted oil wells connected to a manifold located at seabed, which in turn is connected to a booster-pump and a transportation line to a top side facility. A depiction of the system is given in figure 3.1.

Each oil well is equipped with a downhole ESP, which utilize a powerful, high grade electrical motor to drive a multistage centrifugal pump. The purpose of the ESP is to increase the pressure in the well to overcome the sum of pressure losses along the flow path from bottom hole to the well head. The ESP system is driven by a variable frequency generator (VFG) which enables the operator to control the differential pressure exerted by the pump by adjusting the mechanical frequency of the current.

At seabed, a manifold connects all the wells and a water valve together. Each well is connected to the manifold through a choke (i.e., a control valve) located at the well head, which enables control of flow from the well into the manifold. A water valve is connected to the manifold to supply water to the produced fluid to ensure a total water cut above a certain threshold. High water cut is necessary to keep the viscosity of the

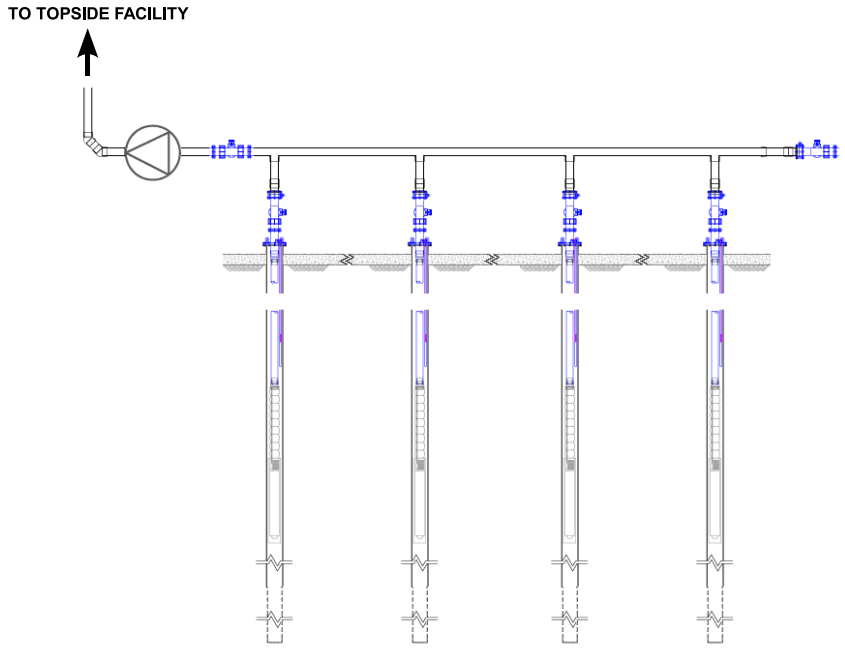

Figure 3.1: A depiction of the complete system with four ESP lifted wells connected to a common manifold. The manifold is connected to a booster-pump, which in turn is connected to a transportation line. Water is fed into the manifold through the valve on the right.

produced fluid at a low level.

Further, the manifold is connected to a booster pump which relay the produced fluid from the manifold to a transportation line that rise from the seabed to a topside facility. The booster-pump serve the same purpose as the downhole ESP, which in this context is to increase the pressure at the entry point of the transportation line to overcome pressure losses along the transportation line.

It is useful to consider the complete system as a series of interconnected modules, where each module represent a physical unit. Utilizing

this mentality, a mathematical model for the complete system can be derived by constructing models for each of the different parts independently in a sequential manner.

The most complex module in the system is the well itself and thus, a mathematical model for this module is constructed first. Modeling of the well is treated in section 3.2. In order to complete the well model derived in section 3.2, models for the downhole ESP and friction forces in the system are required. Modeling aspects related to these components are dealt with in section 3.3 and 3.4, respectively.

The well interact with its environment through a reservoir located at the well bottom and the wellhead choke, represented by boundary conditions. Reservoir and choke models are presented in section 3.5. In turn, models for the manifold, booster-pump and transportation line are presented in section 3.6.

To summarize the modeling procedure, the complete simulation model is presented in section 3.7

3.2 Well Model

The well is modeled as a hydraulic transmission line where the whole length of the well is divided into a series of interconnected control volumes. The pressure and flow through each control volume are influenced by the pressure and flow in the neighboring control volumes. A general modeling approach of a hydraulic transmission line is presented in section 3.2.1.

The model derived in section 3.2.1 are then discretized by assuming that the well is spatially discretized into a finite set of control volumes. The discrete model is presented in section 3.2.2.

3.2.1 Hydraulic transmission line

The model for a hydraulic transmission line presented in this section is derived in Egeland and Gravdahl [2003, p. 429]. The text given in this section is in close resemblance to that presented in the reference.

A hydraulic transmission line is a pipe of cross section A and length L with a compressible fluid. The dynamic model for the transmission line is developed from the mass and momentum balance of a differential control volume Adx where A is the cross section area of the pipe and x is the length coordinate along the pipe. It is assumed that the density of the

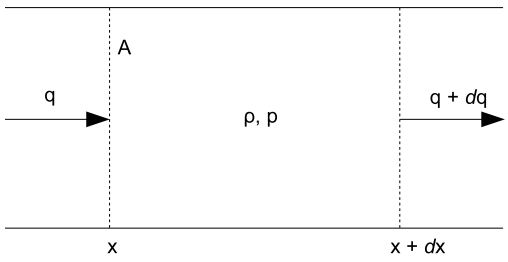

Figure 3.2: Volume element for hydraulic transmission line

fluid is not varying over the cross section, so that $\rho = \rho(x,t)$. The mass flow is

$$w(x,t) = \int_A \rho v dA = \rho \bar{v} A \tag{3.1}$$

where $\bar{v}$ is the average velocity. The mass balance is taken from the fixed differential control volume Adx from x to $x + dx$. The mass flow into the volume is w at x, while the mass flow out of the volume is $w + dw$ at $x + dx$. An illustration of a single control volume is given in figure 3.2 . The mass balance is then found from (3.1) to be

$$Adx\frac{\delta \rho}{\delta t} = w - (w + dw) = -dw$$

Divide by Adx and we get

$$\frac{\delta \rho}{\delta t} = -\frac{1}{A}\frac{\delta w}{\delta x}$$

A change of variables from density ρ to pressure p is achieved in the mass balance using the constitutive equation $dp = (\beta/\rho)dp$ where β is the bulk modulus of the fluid. This gives

$$\frac{\delta p}{\delta t} = -\frac{\beta}{\rho A}\frac{\delta w}{\delta x}$$

The momentum equation is found from Egeland and Gravdahl [2003, Eq. (11.63)]

$$\frac{\delta}{\delta t}(\rho \bar{v})Adx = Ap - A(p+dp) + \int_A \rho v^2 dA - \int_A [\rho v^2 + d(\rho v^2)]dA - Fdx \tag{3.2}$$

where Fdx is the friction force. This gives

$$\frac{\delta w}{\delta t} = -A\frac{\delta p}{\delta x} - A\frac{\delta}{\delta x}\int_A \rho v^2 dA - F$$

We will assume that the average velocity $\bar{v}$ is close to zero, so the second term on the right hand side can be set to zero ($v^2 \approx 0$). The model becomes

$$\begin{aligned}\frac{\delta p}{\delta t} &= -\frac{\beta}{\rho A}\frac{\delta w}{\delta x} \\ \frac{\delta w}{\delta t} &= -A\frac{\delta p}{\delta x} - F\end{aligned}$$

These equations are usually formulated in terms of the pressure p and the volumetric flow q by treating the density as a constant ρ_0 such that $w = \rho_0 q$. The transmission line model linearized around $q = 0$ and $\rho = \rho_0$ is given by

$$\frac{\delta p}{\delta t} = -\frac{\beta}{A}\frac{\delta q}{\delta x} \tag{3.3}$$

$$\frac{\delta q}{\delta t} = -\frac{A}{\rho_0}\frac{\delta p}{\delta x} - \frac{F}{\rho_0} \tag{3.4}$$

The flow model in (3.4) is only valid for horizontal transmission lines. In order to apply the model to vertical transmission lines, an additional term that represents loss in hydrostatic pressure must be added. Thus, a model for a vertical hydraulic transmission line is given according to

$$\begin{aligned}\frac{\delta q}{\delta t} &= -\frac{A}{\rho_0}\frac{\delta p}{\delta x} - \frac{F}{\rho_0} - \frac{A\rho_0 g}{\rho_0}\frac{\delta h}{\delta x} \\ &= -\frac{A}{\rho_0}\frac{\delta p}{\delta x} - \frac{F}{\rho_0} - Ag\frac{\delta h}{\delta x}\end{aligned} \tag{3.5}$$

where the last term on the right hand side represent loss in hydrostatic pressure

3.2.2 Discretization

The model for vertical transmission lines given by (3.3) and (3.5) describe the change in pressure and flow in an infinitesimal control volume, over an

infinitesimal time interval. In order to implement the model on a computer it needs to be discretized in both time and space.

Spatially discretization is achieved by dividing the overall length of the well into a finite set of control volumes. It is useful to treat the well segment between the reservoir and the ESP unit separately from the well segment between the ESP unit and the choke. To be precise, the lower well segment is divided into m different control volumes, while the upper well segment is divided into n different control volumes. The concept is illustrated in figure 3.3.

Notice that the boundary conditions are given as input to control volume 1 and output from control volume $m + n$. The downhole ESP unit is modeled as a change in boundary conditions between its neighboring control volumes. In this respect, it is assumed that the ESP has infinitesimal height and that it exert an instantaneous pressure differential Δp_{ESP} between the neighboring control volumes.

Discrete model By assuming that the well is devided into $m+n$ different control volumes, the dynamics of the well are explained by the following set of differential equations.

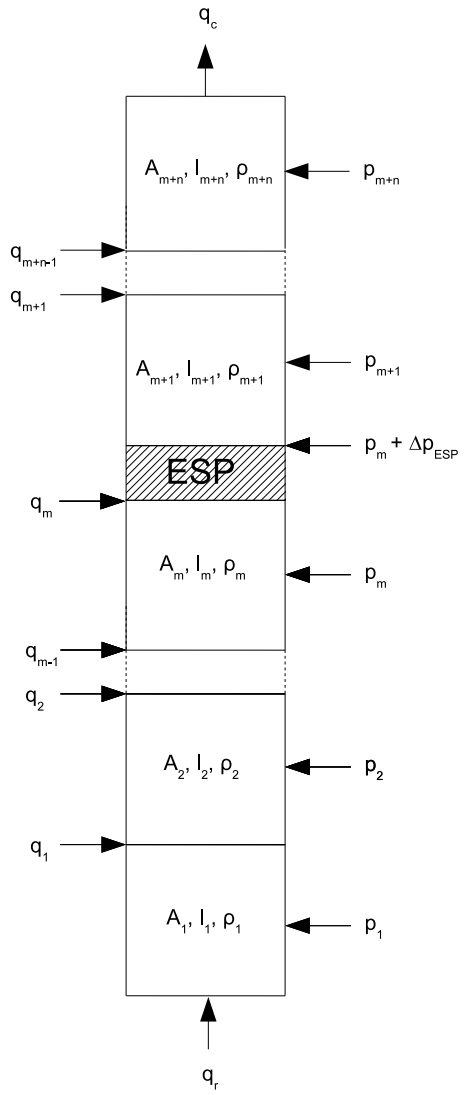

Figure 3.3: Spatially discretization into a finite number of control volumes. Boundary conditions are given as input to and output from the outer control volumes. Notice the pressure differential Δp_{ESP} across the ESP.

$$\dot{p}_1 = \frac{\beta_1}{V_1}(q_r - q_1) \tag{3.6}$$

$$\dot{q}_1 = \frac{A_1}{\rho_1 l_1}(p_1 - p_2) - \frac{F_1}{\rho_1 l_1} - \frac{A_1 g}{l_1}(h_r - h_1) \tag{3.7}$$

$$\dot{p}_2 = \frac{\beta_2}{V_2}(q_1 - q_2) \tag{3.8}$$

$$\dot{q}_2 = \frac{A_2}{\rho_2 l_2}(p_2 - p_3) - \frac{F_2}{\rho_2 l_2} - \frac{A_2 g}{l_2}(h_1 - h_2) \tag{3.9}$$

$$\vdots$$

$$\dot{p}_m = \frac{\beta_m}{V_m}(q_{m-1} - q_m) \tag{3.10}$$

$$\dot{q}_m = \frac{A_m}{\rho_m l_m}(p_m - p_{m+1}) - \frac{F_m}{\rho_m l_m} - \frac{A_m g}{l_m}(h_m - h_{m+1}) \tag{3.11}$$

$$\dot{p}_{m+1} = \frac{\beta_{m+1}}{V_{m+1}}(q_m - q_{m+1}) \tag{3.12}$$

$$\dot{q}_{m+1} = \frac{A_{m+1}}{\rho_{m+1} l_{m+1}}((p_{m+1} + \Delta p_{ESP}(f_{ESP})) - p_{m+2}) - \frac{F_{m+1}}{\rho_{m+1} l_{m+1}} - \frac{A_{m+1} g}{l_{m+1}}(h_{m+1} - h_{m+2}) \tag{3.13}$$

$$\vdots$$

$$\dot{p}_{m+n} = \frac{\beta_{m+n}}{V_{m+n}}(q_{m+n-1} - q_{m+n}) \tag{3.14}$$

$$\dot{q}_{m+n} = \frac{A_{m+n}}{\rho_{m+n} l_{m+n}}\left(p_{m+n} - p_c^{in}\right) - \frac{F_{m+n}}{\rho_{m+n} l_{m+n}} - \frac{A_{m+n} g}{l_{m+n}}(h_{m+n} - h_c) \tag{3.15}$$

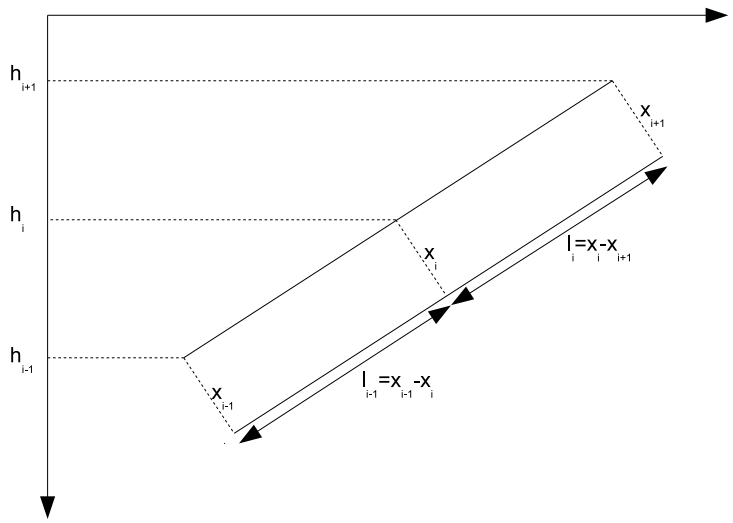

Figure 3.4: The height and length of a control volume are different from each other when the well has a horizontal component. Notice that $l_i = x_i - x_{i+1}$ converge to $h_i - h_{i+1}$ if the horizontal component is non-existing.

The subscripts indicate which control volume the equations and parameters apply to. Each control volume is characterized by the following set of parameters: cross-section A_i, length $l_i = x_{i+1} - x_i$, fluid density ρ_i, friction force F_i and a height h_i representing the vertical height of the control volume. The height of a control volume deviate from the length if the well is drilled with a horizontal component, as shown in figure 3.4. Notice that the volume is given by $V_i = A_i l_i = A_i(x_{i+1} - x_i)$. The outer control volumes, i.e., control volume 1 and $m + n$, incorporate the reservoir height h_r and choke height h_c which represents the delimitations of the well. Subscript denoting the time instance are omitted for simplicity.

3.3 Electrical submersible pump

3.3.1 Background

An ESP unit is often realized as an electrically driven centrifugal pump. The centrifugal pump is normally designed as a multistage pump, meaning that the total pressure increase over the pump is obtained as the increment of minor pressure increases across each stage. Often the ESP unit is equipped with a variable frequency generator (VFG) which enables the

ESP to be run at different frequencies. Such ESP units enables variable frequency drive (VFD) which is a important feature that allow accurate control of the throughput from the pump.

The performance of an ESP is dependent on the properties of the fluid passing through the pump and the differential pressure developed by the pump. The performance of ESPs is often specified in terms of head units H where the head produced by the ESP is defined as

$$H_{ESP}(f_{ESP}) = \frac{\Delta p_{ESP}(f_{ESP})}{\rho g} \tag{3.16}$$

where Δp_{ESP} is the differential pressure exerted by the ESP. Here, f_{ESP} signify that H_{ESP} and Δp_{ESP} is dependant of the mechanical frequency of the current running the ESP unit.

An expression for Δp_{ESP} is obtained by rearranging (3.16)

$$\Delta p_{ESP}(f_{ESP}) = \rho_m g H_{ESP}(f_{ESP}) \tag{3.17}$$

The head-flow characteristics for a selected frequency is often provided by the manufacturer. The characteristic is a performance indicator for the ESP and is used in the model deduction for the unit. The head-flow-characteristic can be extended to different frequencies by use of the *affinity laws* defined by

$$\frac{q_1}{q_0} = \left(\frac{f_1}{f_0}\right) \quad and \quad \frac{H_1}{H_0} = \left(\frac{f_1}{f_0}\right)^2$$

where H_0 is a known head-flow characteristic for a given frequency f_0. To illustrate how a typical head-flow characteristic is effected by the affinity laws example 3.1 is constructed. The ESP characteristic used in this thesis is similar to the H_0 characteristic from example 3.1.

Example 3.1 *Suppose that the head-flow-characteristics H_0 for a selected frequency $f_0 = 40Hz$ are approximated by the polynomial*

$$H_0(q) = -3.56 \cdot 10^7 q^4 + 1.88 \cdot 10^6 q^3 - 3.68 \cdot 10^4 q^2 + 17q + 21,$$

and that the corresponding characteristic for the frequencies $f_1 = 45Hz$ and $f_2 = 35Hz$ are desired.

According to the affinity laws these characteristics are given by

$$\begin{aligned} H_1 &= H_0 \left(\frac{f_1}{f_0} \right)^2 = H_0 \cdot 1.125^2 \\ H_2 &= H_0 \left(\frac{f_2}{f_0} \right)^2 = H_0 \cdot 0.875^2 \end{aligned}$$

and

$$\begin{aligned} q_1 &= q \left(\frac{f_1}{f_0} \right) = q \cdot 1.125 \\ q_2 &= q \left(\frac{f_{12}}{f_0} \right) = q \cdot 0.875 \end{aligned}$$

A graphical comparison of the three different head-flow characteristics are provided in figure 3.5.

△

3.3.2 Operational constraints

Each ESP unit is delivered with a set of operational guide lines provided by the manufacturer. These guide lines include performance parameters belonging to the best efficiency point (BEP) represented by a criteria for an optimum utilization of the pump, and recommended range of operation about the BEP. The recommended operation area is known as the *operational envelope.*

The recommended range of operation for any ESP is strictly related to axial forces occuring in the pump. Static and dynamic axial forces occurring in pump stages are the result of different phenomena existing in downthrust and upthrust. The axial forces deterioratate the efficiency of the pump and cause wear and tear that leads to mechanical damage of the stages.

Keeping the operation of an ESP unit inside the recommended oper-

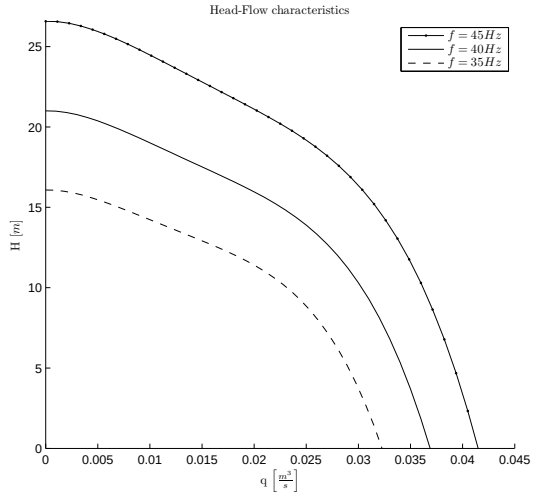

Figure 3.5: A comparison of head-flow characteristics for three different ESP frequencies.

ational envelope poses severe restriction in the application of ESP equipment. Due to large expenses related to maintanence and replacement of installed ESP units it is important that the expected lifetime of the pump is kept as large as possible, and this is ensured by keeping the ESP within its operational envelope.

3.3.3 Implementation aspects

The planned location of the ESP in the well model is between control volume m and $m+1$, as illustrated in figure 3.3. To easily identify the intake and discharge pressure from the ESP, the following notation is introduced

$$p_{ESP}^{in} = p_m \tag{3.18}$$

$$\begin{aligned} p_{ESP}^{out} &= p_{m+1} \\ &= p_m + \Delta p_{ESP}(f_{ESP}) \end{aligned} \tag{3.19}$$

The centrifugal pump in the ESP contain an impeller, a rotating mechanical device with a moment of inertia and limitations on rate of change in angular velocity. The angular velocity of the impeller is determined by the mechanical frequency of the current driving the ESP and so, limitations on change in angular velocity can be expressed as limitations on rate

of change in frequency

$$\begin{aligned} \dot{f}_{ESP} &= sat(\dot{f}_{ESP}) \\ &= \begin{cases} \dot{f}_{ESP}, & if\ |\dot{f}_{ESP}| \leq \dot{f}_{ESP}^{max} \\ sgn(\dot{f}_{ESP})\dot{f}_{ESP}^{max}, & if\ |\dot{f}_{ESP}| > \dot{f}_{ESP}^{max} \end{cases} \end{aligned} \tag{3.20}$$

where $sgn(\cdot)$ is the signum function.

3.4 Modeling friction

The fiction model is composed of two components; friction arising from shear stress, and friction from geometric restrictions in the well.

3.4.1 Shear stress

When a fluid moves through a well, tangential forces arise between the fluid and the inner surface of the well. The tangential forces are referred to as the wall shear stress and are defined according to

$$\tau_w = \frac{F_w}{A_w}$$

where F_w is the friction force and A_w represent the surface area of the wall. In a fully developed, smooth pipe flow, McKeon et al. [2005] suggest that the friction factor λ can be used to express τ_w according to

$$\lambda = \frac{4\tau_w}{\frac{1}{2}\rho v^2},$$

and that λ can be approximated using Blasius's correction factor given by

$$\lambda = \frac{0.3164}{Re^{0.25}}$$

where the Reynolds number $Re = \frac{\rho v d}{\mu}$. Here, ρ is the fluid density, v is the fluid velocity, d is the diameter of the well and μ is the dynamic viscosity.

Combinding these two different expressions for λ, τ_w can be expressed by

$$\begin{aligned} \tau_w &= 0.0791 Re^{-0.25} \frac{\rho v^2}{2} \\ &= 0.0791 Re^{-0.25} \frac{\rho}{2} \left(\frac{q}{A}\right)^2 \end{aligned} \tag{3.21}$$

Based on the previous expression for τ_w the friction force F_w can be found using the definition of the wall shear stress

$$\begin{aligned} F_w &= A_w \tau_w \\ &= (xS_w)\tau_w \end{aligned}$$

where $S_w = d\pi$ is the perimeter of the well and x the height of the well segment. Inserting τ_w from (3.21) yield

$$F_w = (xS_w) \cdot 0.0791 Re^{-0.25} \frac{\rho}{2} \left(\frac{q}{A}\right)^2$$

F_w for a control volume with infinitesimal height δx are then expressed according to

$$\frac{\delta F_w}{\delta x} = 0.0791 S_w Re^{-0.25} \frac{\rho}{2} \left(\frac{q}{A}\right)^2 \tag{3.22}$$

3.4.2 Geometric restrictions

In addition to friction between the surface of the well and the fluid moving through it, friction occurs when fluid flow through geometric restrictions in the well. The magnitude of this friction force is usually significantly less than F_w and thus refered to as F_{minor}. White [2008, p. 383] propose that a pressure loss Δp over a geometric restriction can be approximated by

$$\Delta p = K \frac{\rho v^2}{2} = K \frac{\rho}{2} \left(\frac{q}{A}\right)^2$$

from which the friction force F_{minor} can be derived by multiplying the pressure loss with the cross-section area A of the well

$$\begin{aligned} F_{minor} &= A\Delta p \\ &= AK \frac{\rho}{2} \left(\frac{q}{A}\right)^2 \end{aligned}$$

where K is a dimensionless loss coefficient.

For an well segment of infinitesimal height δx the friction loss become

$$\frac{\delta F_{minor}}{\delta x} = A \frac{\delta K}{\delta x} \frac{\rho}{2} \left(\frac{q}{A}\right)^2 \tag{3.23}$$

where $\frac{\delta K}{\delta x}$ are the gradient of the loss coefficient.

3.4.3 Friction model

The total friction force for a control volume of infinitesimal height become

$$\frac{\delta F}{\delta x} = \frac{\delta F_{minor}}{\delta x} + \frac{\delta F_w}{\delta x}$$

The total friction loss in a control volume with height l is found by integration

$$\begin{aligned} F &= \int_l \left(\frac{\delta F_{minor}}{\delta x} + \frac{\delta F_w}{\delta x} \right) dx \\ &= \int_l \left(A \frac{\delta K}{\delta x} \frac{\rho}{2} \left(\frac{q}{A} \right)^2 + 0.0791 S_w Re^{-0.25} \frac{\rho}{2} \left(\frac{q}{A} \right)^2 \right) dx \\ &= (B_0 + B_1) \frac{\rho q^2}{2} \end{aligned} \tag{3.24}$$

where

$$B_0 = \int_l \frac{\delta K}{\delta x} \frac{1}{A} dx \tag{3.25}$$

$$B_1 = 0.0791 S_w Re^{-0.25} \int_l \frac{1}{A^2} dx \tag{3.26}$$

3.5 Reservoir and wellhead choke

3.5.1 Reservoir model

A well and a productive formation (reservoir) are interconnected at the sandface, a cylindrical surface where the reservoir is breached. A well starts to produce when the pressure at the sandface is less than the reservoir pressure. The pressure at the sandface is in turn determined by the bottom hole pressure.

Takacs [2009] propose a simple approach to relate the flow bottom hole pressure[1] p_{FBHP} to the flow rate q_r from the reservoar by use a productivity index. The productivity index PI is a collection of different parameters that relates the production rate to the difference in reservoar pressure p_r and p_{FBHP}. Takacs [2009, Eq. (2.1) - (2.2)] suggest the following definition of PI

[1] *Flow bottomhole pressure* and *bottomhole pressure* are different terms used to describe the pressure in the lowest part of the well.

$$PI = \frac{0.00708\kappa h}{\mu B ln\left(\frac{r_e}{r_w}\right)}$$

where

κ	-	effective permeability
h	-	pay thickness
B	-	liquid volume factor
r_e	-	drainage radius of the well
r_w	-	radius of the wellbore

From this the reservoar flow q_r is expressed according to

$$\begin{aligned} q_r &= \frac{0.00708\kappa h}{\mu B ln\left(\frac{r_e}{r_w}\right)}(p_r - p_{FBHP}) \\ &= PI(p_r - p_{FBHP}) \end{aligned} \tag{3.27}$$

3.5.2 Control valve

The flow from each well to the manifold is managed by a control valve located at the wellhead. The control valve is often referred to as the *choke* and it is an important part of the wellhead.

A common way to model the flow q_c through the choke is to relate the flow to the differential pressure across the choke. White [2008, p. 15] suggest the following relation

$$\begin{aligned} q_c &= C_v\left(\frac{p_c^{in} - p_c^{out}}{SG}\right)^{1/2} \\ &= kG_c(z_c)\sqrt{p_c^{in} - p_c^{out}} \end{aligned} \tag{3.28}$$

where

C_v	-	valve flow coefficient
SG	-	spesific gravity of the fluid
k	-	valve constant
$G_c(z_c)$	-	valve characteristics
z_c	-	valve position

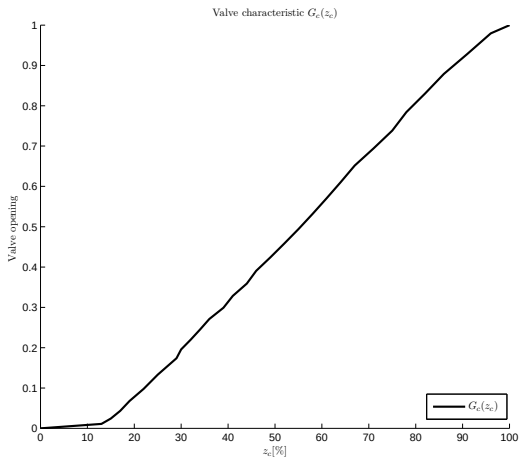

Figure 3.6: Graphical representation of the valve characteristic $G_c(z_c)$. The ordinate axis represent fractional valve opening (0 - closed, 1 - fully open).

The valve constant k is a composition of unknown parameters. The valve characteristic $G_c(z_c) \in [0, 1]$ is a function describing the fractional valve opening as a function of valve position $z_c \in [0, 100]$. A graphical representation of the valve characteristic used throughout this thesis is given in figure 3.6.

3.5.3 Implementation aspects

The reservoir flow q_r act as a boundary condition to control volum 1 in the well model from figure 3.3. q_r is computed from (3.27) as a function of $p_{_{FBHP}}$ and, using figure 3.3 as basis, the following change of notation is introduced

$$p_{_{FBHP}} = p_1$$

The choke is located at the top of the well and is thus connected to control volume $m + n$ in the well model from figure 3.3. To easily identify the choke input pressure p_c^{in} as the pressure at the top of the well, the following change of notation is beneficial

$$p_c^{in} = p_{m+n}$$

The choke connects the well to the manifold and so, the choke output pressure p_c^{out} is the same as the manifold pressure p_{man}, i.e.,

$$p_c^{out} = p_{man}$$

In reality, a change in choke position z_c involve physical movement of mechanical parts and this suggests that limitations on rate of change in z_c should be imposed. In a same manner as for ESP frequency f_{ESP}, rate limitations on z_c are given by

$$\begin{aligned} \dot{z}_c &= sat(\dot{z}_c) \\ &= \begin{cases} \dot{z}_c, & if\ |\dot{z}_c| \leq \dot{z}_c^{max} \\ sgn(\dot{z}_c)\dot{z}_c^{max}, & if\ |\dot{z}_c| > \dot{z}_c^{max} \end{cases} \end{aligned} \tag{3.29}$$

3.6 Modeling the manifold, booster-pump and transportation line

3.6.1 Manifold modeling

The manifold is connected to the wells through a choke at each wellhead and it is designed such that it accumulate produced liquid q_c^i from the $i = 1, \cdots, 4$ connected wells. In addition, the manifold is constructed with a water feed that inject a flow of water q_{wv} into the manifold to ensure a high water cut in the total flow from the manifold. The total flow accumulated in the manifold is given by

$$q_{man}^{in} = \sum_{i=1}^{4} q_c^i + q_{wv} \tag{3.30}$$

The manifold pressure p_{man} is derived by treating the manifold as a hydraulic transmission line with a single control volume. In doing so, (3.3) can be applied according to

$$\begin{aligned} \dot{p}_{man} &= \frac{\beta_{man}}{A_{man} l_{man}} \left(q_{man}^{in} - q_{man}^{out} \right) \\ &= \frac{\beta_{man}}{V_{man}} \left(q_{man}^{in} - q_{man}^{out} \right) \end{aligned} \tag{3.31}$$

where A_{man} is the manifold cross-section area, l_{man} is the manifold length and V_{man} is the manifold volume.

3.6.2 Model for the booster-pump

The manifold is connected to the subsequent transportation line through a booster-pump. The purpose of the booster-pump is to increase the pressure at the entry point of the transportation line to overcome pressure loss along the transportation line.

The pressure increase $\Delta p_{_{BP}}$ attained by the booster-pump is modeled in the same manner as the ESP from (3.17) according to

$$\Delta p_{_{BP}}(f_{_{BP}}) = \rho_{man} g H_{_{BP}}(f_{_{BP}}) \tag{3.32}$$

where $H_{_{BP}}(f_{_{BP}})$ is the head exerted by the pump at a given frequency $f_{_{BP}}$. The reader is referred to section 3.3 for modeling details.

3.6.3 Transportation line modeling

The transportation line is modeled as a hydraulic transmission line with a single control volume. Since the pressure in both ends of the control volume is explicitly given by the discharge pressure from the booster-pump and the topside pressure condition $p_{topside}$, there is no need to derive a model for the pressure in the transportation line. It is only necessary to formulate a model for the flow q_{tr} through the transportation line, and this is achieve using (3.4) according to

$$\dot{q}_{tr} = \frac{A_{tr}}{\rho_{tr} l_{tr}} \left((p_{man} + \Delta p_{_{BP}}) - p_{topside} \right) - \frac{F_{tr}}{\rho_{tr}} \tag{3.33}$$

where A_{tr} is the cross-section area and l_{tr} is the length of the transportation line. The fluid density ρ_{tr} is the same as the in the manifold, i.e., $\rho_{tr} = \rho_{man}$. The friction loss along the transportation line are represented by F_{tr} and is modeled according to (3.24).

3.6.4 Implementation aspects

The booster-pump is modeled in the same manner as an ESP, but without operational constraints. In addition, the booster pump is modeled such that it provides a constant head $H_{_{BP}}$ for a given frequency $f_{_{BP}}$. This is done to circumvent numerical issues when $f_{_{BP}}$ is assigned values outside the normal operation domain of the ESP.

3.7 Simulation model

Mathematical models developed for different parts of the system are merged together in a complete simulation model. The complete model is dependant on the selected number of control volumes and wells. A fairly simple model using two control volumes is used throughout the thesis. The implemented model is presented in section 3.7.1 and 3.7.2.

3.7.1 Two-volume well model

The implemented system incorporate four ESP lifted wells, where each well is constructed using two control volumes as seen from figure 3.7. Thus, each well in the system are represented by the following set of equations

$$\begin{aligned}
\dot{p}_{FBHP} &= \frac{\beta_1}{V_1}\left(q_r - \overline{q}\right) \\
&= \frac{\beta_1}{V_1}\left(PI\left(p_r - p_{FBHP}\right) - \overline{q}\right) && (3.34) \\
\dot{p}_c^{in} &= \frac{\beta_2}{V_2}\left(\overline{q} - q_c\right) \\
&= \frac{\beta_2}{V_2}\left(\overline{q} - kG_c(z_c)\sqrt{p_c^{in} - p_{man}}\right) && (3.35) \\
\dot{\overline{q}} &= \frac{\overline{A}}{\overline{\rho}\overline{l}}\left(p_{FBHP} - p_c^{in} + \Delta p_{ESP}(f_{ESP}) - \frac{\left(B_0^1 + B_1^1\right)}{A_1}\frac{\rho_1\overline{q}^2}{2}\right. \\
&\quad \left. - \frac{\left(B_0^2 + B_1^2\right)}{A_2}\frac{\rho_2\overline{q}^2}{2} - \rho_1 g\left(h_r - h_p\right) - \rho_2 g\left(h_p - h_c\right)\right) && (3.36)
\end{aligned}$$

Instead of calculating the flow through each control volume, an average flow $\overline{q}$ is derived using the average cross-section area $\overline{A} = \frac{A_1+A_2}{2}$, average density $\overline{\rho} = \frac{\rho_1 V_1 + \rho_2 V_2}{V_1+V_2} = \frac{\rho_1(A_1 l_1)+\rho_2(A_2 l_2)}{A_1 l_1 + A_2 l_2}$ and average length $\overline{l} = \frac{l_1+l_2}{2}$ of the two control volumes.

3.7.2 Additional dynamics

The manifold and transportation line are modeled by the following equations

$$\dot{p}_{man} = \frac{\beta_{man}}{V_{man}} \left(q_{man}^{in} - q_{tr} \right) \tag{3.37}$$

$$\dot{q}_{tr} = \frac{A_{tr}}{\rho_{tr} l_{tr}} \left(p_{man} + \Delta p_{_{BP}}(f_{_{BP}}) - p_{topside} - \frac{\left(B_0^{tr} + B_1^{tr} \right)}{A_{tr}} \frac{\rho_{tr} q_{tr}^2}{2} \right) \tag{3.38}$$

The rate limitations on f_{ESP}, z_c and $f_{_{BP}}$ are included according to

$$\dot{f}_{_{ESP}} = \begin{cases} \dot{f}_{_{ESP}}, & if \ |\dot{f}_{_{ESP}}| \leq \dot{f}_{_{ESP}}^{max} \\ sgn(\dot{f}_{_{ESP}}) \dot{f}_{_{ESP}}^{max}, & if \ |\dot{f}_{_{ESP}}| > \dot{f}_{_{ESP}}^{max} \end{cases} \tag{3.39}$$

$$\dot{z}_c = \begin{cases} \dot{z}_c, & if \ |\dot{z}_c| \leq \dot{z}_c^{max} \\ sgn(\dot{z}_c) \dot{z}_c^{max}, & if \ |\dot{z}_c| > \dot{z}_c^{max} \end{cases} \tag{3.40}$$

$$\dot{f}_{_{BP}} = \begin{cases} \dot{f}_{_{BP}}, & if \ |\dot{f}_{_{BP}}| \leq \dot{f}_{_{BP}}^{max} \\ sgn(\dot{f}_{_{BP}}) \dot{f}_{BP}^{max}, & if \ |\dot{f}_{_{BP}}| > \dot{f}_{_{BP}}^{max} \end{cases} \tag{3.41}$$

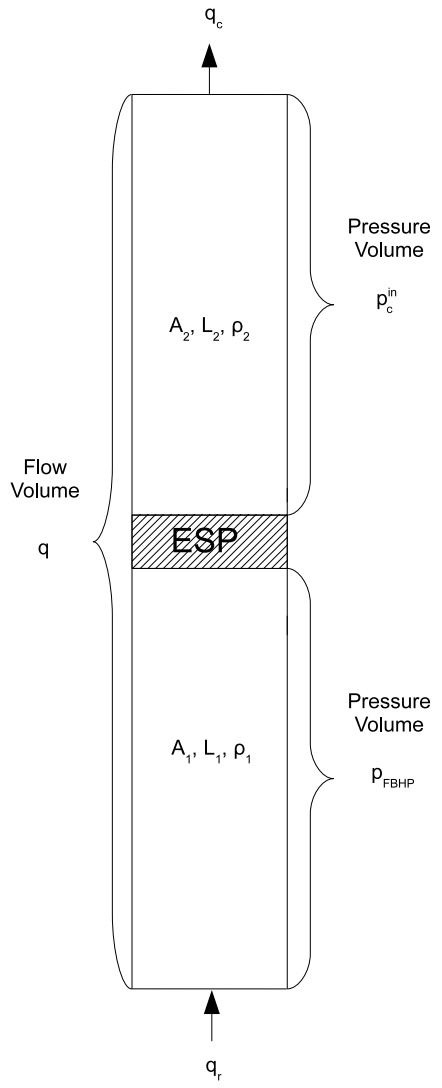

Figure 3.7: The implemented two-volume well model.

Chapter 4

Envelope and Pressure control

4.1 Motivation

This chapter explores the possibility of creating an automatic control system that is able to maintain the ESP operated within a specified safe range of operation. The safe range of operation is defined as the operational envelope and a representation of this is given section 4.2.

The ESP report published by Amundsen et al. [2010] propose a divided control strategy based on two control criteria. The first criteria being envelope control, and the second is control of the flow q through the ESP and pressure Δp_{ESP} exerted by the ESP. The proposed strategy utilize separate control strategies to achieve these criteria. A severe drawback with this control strategy is that it requires use of separate control laws, where the current control strategy is determined using logical enquiries. This control strategy is presented in section 4.3.

The possibility of designing a unified control law that enables both envelope and ESP intake pressure control is investigated in section 4.4.

4.2 Envelope representation

An operational envelope is a set of conditions which define a safe range of operating of the ESP. If the ESP is operated outside this range the unit is subject to excessive wear and tear which limits the life expectancy of the unit and increases the risk of pump failure. It is of vital importance that the ESP unit is operated within its respective operational envelope.

The conditions that form the envelope is given by a minimum and maximum flow $\overline{q}$ through the pump at a particular differential pressure

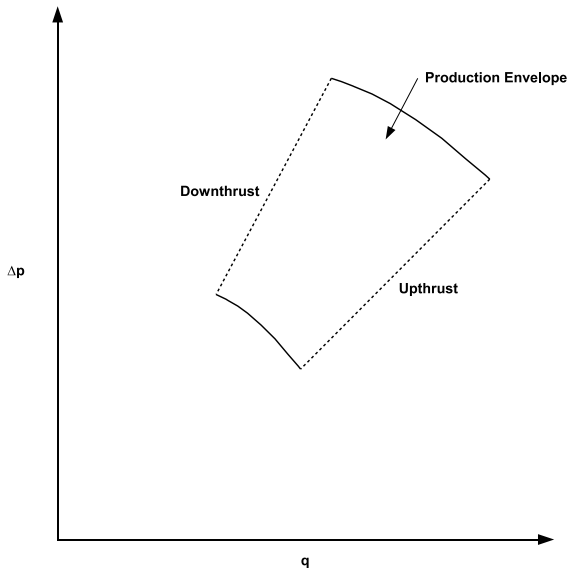

Figure 4.1: The solid lines represent limitations on available pump frequency. The dotted lines represent limitations in flow through the pump. Operation at too high differential pressure and too low flow rate is denoted *downthrust*, while operation at to low differential pressure and too high flow rate is denoted *upthrust*.

Δp_{ESP}, and a minimum and maximum differential pressure Δp_{ESP} for a particular flow $\overline{q}$. A typical operational envelope is shown in figure 4.1.

Upthrust and downthrust conditions It is assumed throughout this thesis that the downthrust and upthrust conditions are represented by stright line segments in a $\overline{q} - \Delta p_{ESP}$ diagram, that can be exactly approximated by the two first order polynomials

$$\Delta p_{ESP}^{D.t.}(\overline{q}) = a^{D.t.}\overline{q} + b^{D.t.} \quad (4.1)$$

$$\Delta p_{ESP}^{U.t.}(\overline{q}) = a^{U.t.}\overline{q} + b^{U.t.} \quad (4.2)$$

where superscript D.t. refer to downthrust and U.t. to upthrust.

Frequency limitations The ESP is limited to operate at a maximum frequency of $65Hz$ and a minimum frequency of $35Hz$. The upper and lower delimitations of the operational envelope are given by the ESP characteristic at the respective frequencies.

4.3 Existing control strategy

The control strategy proposed in the ESP report Amundsen et al. [2010] suggests that separate control strategies should be used to achieve the two control objectives. Amundsen et al. [2010] suggest that one control strategy should be used when the ESP unit is operated outside the envelope, and another control strategy when the ESP is operated inside the envelope. At each time instance only one of the two control schemes is active.

4.3.1 Envelope control

The envelope control problem is solved using a control scheme based on a set of logical enquiries, where the current control law is determined by evaluating the location of the current operating point $(\overline{q}, \Delta p_{_{ESP}})$ with respect to the envelope. Whenever an ESP is operated outside the envelope, the current operating point is located in one of the eight distinct regions shown in figure 4.2. Each of these regions is linked with a control law that enforce necessary action to ensure that the operation of the ESP is brought back inside the envelope.

The control laws associated with the eight regions incorporate use of one or both of the available control inputs $f_{_{ESP}}$ and z_c, according to

$$
\begin{array}{lllllll}
\textit{Region } 1: & f_{_{ESP}} & = & 35, & z_c & = & 100 \\
\textit{Region } 2: & & & & z_c & = & 100 \\
\textit{Region } 3: & f_{_{ESP}} & = & 65, & z_c & = & 100 \\
\textit{Region } 4: & f_{_{ESP}} & = & 65, & & & \\
\textit{Region } 5: & f_{_{ESP}} & = & 65, & z_c & = & 0 \\
\textit{Region } 6: & & & & z_c & = & 0 \\
\textit{Region } 7: & f_{_{ESP}} & = & 35, & z_c & = & 0 \\
\textit{Region } 8: & f_{_{ESP}} & = & 35, & & &
\end{array}
$$

E.g., if the current operating point of the ESP is located in *Region* 1, the appropriate action is to set the ESP frequency to 35Hz and the choke opening to 100%.

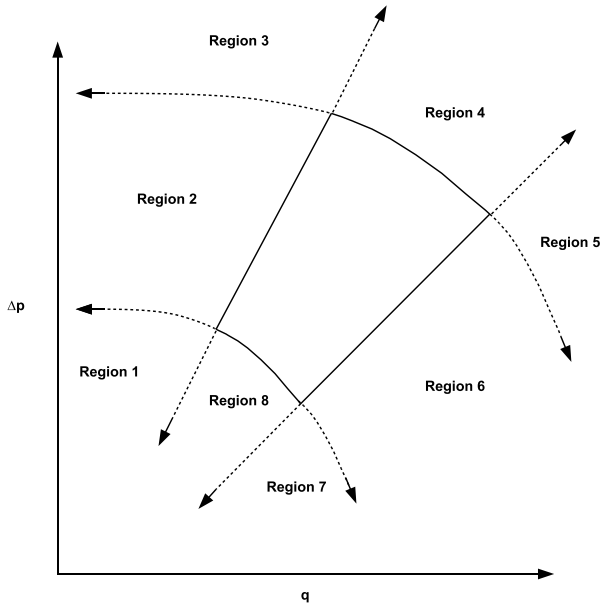

Figure 4.2: The area outside the operational envelope is devided into eight separate regions.

4.3.2 Flow and pressure control

The secondary objective of controlling the flow $\overline{q}$ and differential pressure Δp_{ESP} apply when the ESP is operated within the envelope. In this case, Amundsen et al. [2010] suggest that a standard PI-controller can be used to control Δp_{ESP} with the primary control input f_{ESP}, and that $\overline{q}$ is controlled using a similar controller with the secondary control input z_c. The control laws given in Amundsen et al. [2010, Sec. 8.2.2] are

$$ESP: \quad \begin{aligned} f_{ESP} &= K_{P,ESP} e_{dp} + K_{I,ESP} \int e_{dp} dt \\ e_{dp} &= \Delta p_{ESP}^{SP} - \Delta p_{ESP} \end{aligned}$$

$$Choke: \quad \begin{aligned} z_c &= K_{P,q}, e_q + K_{I,q} \int e_q dt \\ e_{q_{ESP}} &= \overline{q}^{SP} - \overline{q} \end{aligned}$$

where superscript SP denote the desired set-point value.

4.3.3 Concluding remarks

The envelope control scheme presented in 4.3.1 deviates from the control scheme given in Amundsen et al. [2010]. The production envelope in Amundsen et al. [2010] is solely represented by straight line segments, not the curved line segments that represent the ESP characteristics at $35Hz$ and $65Hz$. Consequently, Amundsen et al. [2010] separates the area outside the envelope into a different set of regions than those shown in figure 4.2 and utilize a different set of control laws. Dispite the difference in the control structures, the concept is the same and similar behavior is expected.

4.4 Improved control strategy

One of the main objectives in this thesis is to develop a control system that is capable of controlling the ESP intake pressure to a desired set-point and simultaneously keeping the ESP operated within the envelope. The suggested control system in this section solve the control problem using standard PI-controllers with dynamic saturation limits.

Prior to presenting the control strategy, a discussion on control system requirements and the control objective itself is given in section 4.4.1. Furthermore, the influence from control inputs on the control error is addressed in section 4.4.2.

4.4.1 Control system requirements

An important variable to control in an oil well is the flow rate of the produced fluid. Takacs [2009] state that the best way to control the production rate in an ESP lifted well is to control the ESP intake pressure. In doing so, indirect control of the bottom hole pressure and flow from the reservoir into the well is achieved.

In the simulation model from 3.7, an expression for the ESP intake pressure p_{ESP}^{in} can be derived from physical considerations according to

$$p_{ESP}^{in} = p_c^{in} + \frac{\left(B_0^2 + B_1^2\right)}{A_2}\frac{\rho_2}{2}\bar{q}^2 + \rho_2 g\left(h_p - h_c\right) - \Delta p_{ESP}(f_{ESP}) \qquad (4.3)$$

where the ESP intake pressure is derived as the sum of the choke pressure p_c^{in} and pressure contributions along the flow path from the choke to the ESP. On the right hand side of (4.3), the second term represent pressure increase from friction, the third term account for increase in static pressure, and the fourth term represent pressure increase exerted by the ESP. Note that p_{ESP}^{in} is calculated in a top down-manner, starting from a point at the top of the well.

Equivalently, the ESP intake pressure p_{ESP}^{in} can be derived in a reversed manner, starting from the bottom hole pressure p_{FBHP} and subtracting pressure losses along the flow path to the ESP according to

$$p_{ESP}^{in} = p_{FBHP} - \frac{\left(B_0^1 + B_1^1\right)}{A_2}\frac{\rho_1}{2}q^2 - \rho_1 g\left(h_r - h_p\right)$$

where the second term represent pressure loss from friction, and the third term represent loss of static pressure.

The benefit of using (4.3) to express p_{ESP}^{in} is that there exist an unambigous relationship between the control input f_{ESP}, represented by $\Delta p_{ESP}(f_{ESP})$, and the control variable p_{ESP}^{in}. This relationship is important in determining the influence from f_{ESP} on the control error later on.

The control system must fulfill a number of different requirements stated in the assignment text

- The control system should be able to control p_{ESP}^{in} to a desired set-point $p_{ESP}^{in,SP}$, provided that the production envelope is not violated. If it is not possible to obtain the desired pressure set-point without

violating the envelope constraints, the control error must be minimized to the extent possible while maintaining the ESP operated within the envelope.

- It is desired to use the ESP frequency f_{ESP} as the primary control input and the choke position z_c as the secondary control input. Preferably, only f_{ESP} should be used as control variable and z_c should be kept as high as possible. The preferred choke position is fully open, i.e., z_c at 100%.

4.4.2 Influence from control inputs

Since both control inputs are present in the system dynamics it is not apparent how they should be used to influence the control error $e = p_{ESP}^{in,SP} - p_{ESP}^{in}$. It is important that these connecions are investigated before the control system is designed.

Influence from primary control input The primary control input f_{ESP} directly effect the differential pressure Δp_{ESP} extered by the ESP, where an increase in f_{ESP} cause an increase in Δp_{ESP}. However, by altering f_{ESP} one does not only observe a change in Δp_{ESP} but in other system variables as well. Since Δp_{ESP} is embedded in the flow dynamics (as seen from (3.36)), a change in Δp_{ESP} causes a change in q. Furthermore, q is embedded in the remaining dynamic equations, so all in all, a change in Δp_{ESP} cause changes in all the states of the system.

Due to the extent of dependency in the system there it not exist any clear mathematical expression that explains the exact effect on p_{ESP}^{in} from a change in f_{ESP}. However, simulation results supports that the overall effect from an increase in f_{ESP} is a decrease in p_{ESP}^{in}, and vice versa. This effect is illustrated in figure 4.3.

Influence from secondary control input The secondary control input z_c is embedded in the flow dynamics through the valve characteristic $G_c(z_c)$. By using (3.35) as basis, mathematical reasoning supports that a decrease in choke position imply an increase in p_c^{in} and indirectly, a pressure increase throughout the whole length of the well.

The exact effect from a change in z_c on the control variable p_{ESP}^{in} is unclear from a mathematical point of view and one must apply simulations in order to determine the overall effect. Simulation results support that the

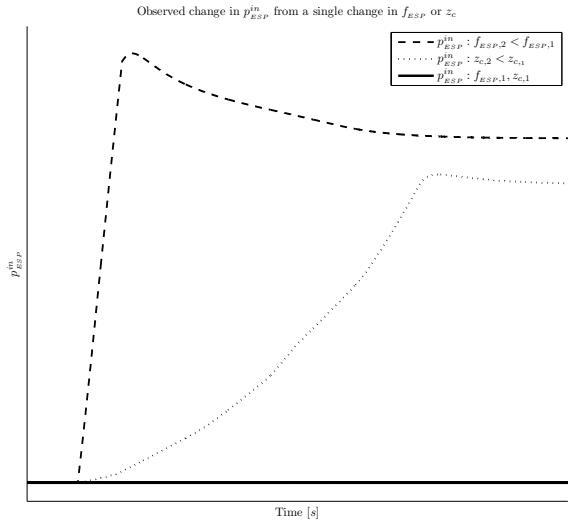

Figure 4.3: The dotted line display the observed effect on p^{in}_{ESP} from a change in f_{ESP}, the striped line display the observed effect on p^{in}_{ESP} from a change in z_c and the solid line dispay normal response without change in f_{ESP} or z_c.

dominating effect from an increase in z_c is a decrease in $\overline{q}$, and consequently an increase in p^{in}_{ESP}, and vice versa. This is also illustrated in figure 4.3.

Input adjustment The previous paragraphs provide a clear understanding of how both control inputs should be used in order to influence p^{in}_{ESP} and thereby the control error. To summarize

- If $e = p^{in,SP}_{ESP} - p^{in}_{ESP} > 0$ then p^{in}_{ESP} is too low and needs to be increased. This could be achieved by either decreasing f_{ESP} or z_c.
- If $e = p^{in,SP}_{ESP} - p^{in}_{ESP} < 0$ then $p^{in}_{ESP}$is too high and needs to lowered. This could be achieved in the opposite way, by increasing f_{ESP} or z_c.

This way of adjusting the control inputs to obtain the desired effect on p^{in}_{ESP} is fundamental in the controller design presented in section 4.4.3.

4.4.3 Controller selection

The incremental PI-controller proposed in Eikrem et al. [2006] is used throughout this thesis. A discrete time representation of this controller is given by

$$\Delta u_k = K_p \left(e_k - e_{k-1} + \frac{\Delta t}{\tau_i} e_k \right) \tag{4.4}$$

where k denote the time index and Δt the sampling time. K_p and τ_i are the proportional gain and integral time, respectively.

The control error is the deviation in ESP intake pressure p^{in}_{ESP} from a desired set-point $p^{in,SP}_{ESP}$, i.e.,

$$e_k = p^{in,SP}_{p,k} - p^{in}_{p,k} \tag{4.5}$$

In agreement with the suggested input adjustment method in section 4.4.2 the control inputs are influenced by the control law according to

$$f_{ESP,k+1} = f_{ESP,k} - \Delta u_k \tag{4.6}$$
$$z_{c,k+1} = z_{c,k} - \Delta u_k \tag{4.7}$$

4.4.4 Dynamic saturation limits

The operational envelope is taken into consideration by imposing dynamic saturation limitations on the controllers. The dynamic saturation limitations offer an efficient way of dealing with constraints in $\overline{q}$ and Δp_{ESP} given by the envelope.

Flow limitations Limitations in flow $\overline{q}$ through the ESP is given by the downthrust and upthrust constraints. The downthrust and upthrust constraint is represented by the straight line segments given in (4.2) and (4.1)

$$\Delta p^{D.t.}_{ESP}(\overline{q}) = a^{D.t.}\overline{q} + b^{D.t.}$$
$$\Delta p^{U.t.}_{ESP}(\overline{q}) = a^{U.t.}\overline{q} + b^{U.t.}$$

By rearranging (4.2) and (4.1) an expression for maximum and minimum flow are obtained

$$q^{max} = \frac{\Delta p_{ESP} - b^{D.t.}}{a^{D.t.}} \tag{4.8}$$

$$q^{min} = \frac{\Delta p_{ESP} - b^{U.t.}}{a^{U.t.}} \tag{4.9}$$

for a given Δp_{ESP}.

It does noe exist an apparent mathematical relation between the limitations in flow and limitations in choke position z_c. However, simulation results indicate a reduction in flow when z_c is reduced, and vice versa. Utilizing this knowledge the following limitations in z_c can be formulated

$$\overline{q} < q^{min} \rightarrow z_{c,k+1} > z_{c,k} \tag{4.10}$$

$$\overline{q} > q^{max} \rightarrow z_{c,k+1} < z_{c,k} \tag{4.11}$$

These limitations state that if the flow is too low $\left(\overline{q} < q^{min}\right)$ the only valid action is to increase z_c, and if the flow is too high $(\overline{q} > q^{max})$ the only valid action is to decrease z_c.

Frequency limitations The limitations in Δp_{ESP} across the ESP are solely given by the ESP characteristics at 35Hz and 65Hz. The most effective way of handling these constraints is to require

$$35 \leq f_{ESP,k+1} \leq 65$$

Although this constraint ensure that the limitations in Δp_{ESP} are met, a change in f_{ESP} may cause violation the downthrust or upthrust constraint. So, in order to ensure that the flow limitations are met, additional frequency limitations are required. The additional limitations are similar to those imposed on z_c

$$q^{min} \geq q \geq q^{max} \rightarrow f_{ESP,k+1} = f_{ESP,k} \tag{4.12}$$

4.4.5 Additional controller dynamics

In order to satisfy all the control system requirements stated in section 4.4.1 additional control features are required:

- To limit the use of z_c as control input to only those situations where use of f_{ESP} is insufficient, f_{ESP} is required to be in saturation before z_c is activated.
- In those situations where sufficient control is achieved using only f_{ESP} the choke position should be as high as possible. This is achieved by incrementing z_c in situations where f_{ESP} is not saturated.

4.4.6 Complete control structure

The complete control structure presented in section 4.4.3 - 4.4.5 is summarized in algorithm 1 to algorithm 4.

Algorithm 1 Control algorithm

1: $e_k \leftarrow p^{in,SP}_{ESP,k} - p^{in}_{ESP,k}$
2: $\Delta u_k \leftarrow K_p \left(e_k - e_{k-1} + \frac{\Delta t}{\tau_i} e_k \right)$
3: $\left[q^{min}, q^{max} \right] = DynamicSaturationLimits()$
4: $[f_{ESP,k+1}, IsSaturated] = UpdateF_{ESP} \left(f_{ESP,k}, \Delta u_k, q, q^{min}, q^{max} \right)$
5: $[z_{c,k+1}] = UpdateZ_c \left(z_{c,k}, \Delta u_k, q, q^{min}, q^{max}, IsSaturated \right)$

Algorithm 2 DynamicSaturationLimits()

1: $q^{min} \leftarrow \frac{\Delta p_{ESP} - b^{D.t.}}{a^{D.t.}}$
2: $q^{max} \leftarrow \frac{\Delta p_{ESP} - b^{U.t.}}{a^{U.t.}}$
3: **return** $q^{min}, \quad q^{max}$

Algorithm 3 UpdateF$_{ESP}(f_{ESP,k}, \Delta u_k, q, q^{min}, q^{max})$

$f_{ESP,k+1} \leftarrow f_{ESP,k} - \Delta u_k$
if $f_{ESP,k+1} > 65$ **then**
  $f_{ESP,k+1} \leftarrow 65$
else if $f_{ESP,k+1} < 35$ **then**
  $f_{ESP,k+1} \leftarrow 35$
end if
if $q^{min} \leq q \leq q^{max}$ **then**
  IsSaturated $\leftarrow 0$
else
  IsSaturated $\leftarrow 1$
  $f_{ESP,k+1} \leftarrow f_{ESP,k}$
end if
return $f_{ESP,k+1}$, IsSaturated

Algorithm 4 UpdateZ$_c(z_{c,k}, \Delta u_k, q, q^{min}, q^{max}$, IsSaturated)

if IsSaturated $= 1$ **then**
  $z_{c,k+1} \leftarrow z_{c,k} - \Delta u_k$
else
  $z_{c,k+1} \leftarrow z_{c,k} + 1$
end if
if $q < q^{min}$ **then**
  $z_{c,k+1} \leftarrow z_{c,k} + 1$
else if $q > q^{max}$ **then**
  $z_{c,k+1} \leftarrow z_{c,k} - 1$
end if
return $z_{c,k+1}$

Control structure	K_p	τ_i	τ_d
P	$0.5K_{p,critical}$	∞	0
PI	$0.5K_{p,critical}$	$0.85T_{critical}$	0
PID	$0.6K_{p,critical}$	$0.5T_{critical}$	$0.12T_{critical}$

Table 4.1: Ziegler-Nichols tuning parameters. With a proportional gain $K_{p,critical}$, a sustained oscillation with a period of $T_{critical} = \frac{1}{f_{critical}}$ is observed.

4.4.7 Controller tuning

The control system derived in the previous sections is tuned to obtain desired closed-loop behavior. The applied tuning procedure is the well known *Ziegler-Nichols Method* which can be used on inherently stable systems. The method involve an experimental approach to deriving the desired controller parameters where the proportional gain K_p is gradually increased until a stationary oscillation is observed on the process output when a small disturbance actuates the system. In this instance, the value of the proportional gain is denoted $K_{p,critical}$. The proportional gain $K_{p,critical}$ and the period of the oscillation $T_{critical} = \frac{1}{f_{critical}}$ form the basis from which the tuned controller parameters are derived. The integral (and derivative) action is put out of action during the tuning procedure by selecting $\tau_i \approx \infty$ (and $\tau_d = 0$). The tuned controller parameters are selected according to table 4.1.

The control system have been tuned using the Ziegler-Nichols procedure with a disturbance represented by a minute change in the process set-point $p_p^{in,SP}$ in the range of $10^{-2}\,bar$. Simulation results for a set of carefully selected values of K_p are given in figure 4.4, and the results clearly indicate that the critical gain $K_{p,critical}$ is within the domain of $0.31 \leq K_p \leq 0.33$, and somewhat close to $K_p = 0.32$. The frequency of the oscillation is close to $f_{critical} = 2\ Hz$, which gives a critical period of $T_{critical} = \frac{1}{f_{critical}} = 0.5\ s$.

By using $K_{p,critical} = 0.32$ and $T_{critical} = 0.5$ for a the PI-controller in

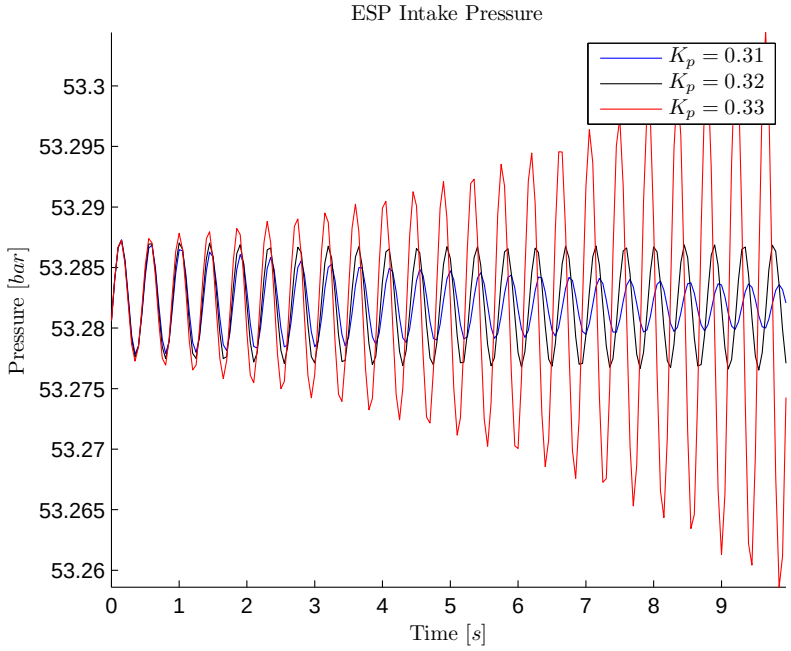

Figure 4.4: Simulation in closed-loop with a proportional gain $K_p = 0.32$ result in a slowly decaying oscillation on the process output p_p^{in}. A minor gain increase to $K_p = 0.33$ yield an oscillation with increasing amplitude on the output, and a minor decrease to $K_p = 0.31$ yield a decreasing oscillation.

table 4.1, the proportional gain and integral time become

$$\begin{aligned} K_p &= 0.5K_{p,critical} \\ &= 0.5 \cdot 0.32 \\ &= 0.16 \\ \tau_i &= 0.85T_{critical} \\ &= 0.8 \cdot 0.5 \\ &= 0.4 \end{aligned}$$

These controller parameters are used in the stability analysis in chapter 5 and in simulation of different scenarios in chapter 6.

Chapter 5

System analysis

In order to determine the stability properties of the open-loop system given by the simulation model in section 3.7, the complete system must be taken into consideration. Fortunately, the stability properties of the complete system is determined by the stability properties of the individual wells in the system. This is the case since the other parts of the system is solely dependant of the output from the wells.

The simulation model contain different types of nonlinearities which complicate the use of standardized analytical tools for nonlinear systems. In order to perform stability analysis of the system it is deemed necessary to linearize the system and apply linear analytical methods.

Linearization of the system is presented in section 5.1.1 and proof of open-loop stability is derived in section 5.2.1. Open-loop stability of the linearized system is related to stability properties of the nonlinear system in section 5.2.2.

Closed-loop stability of the linearized system is investigated in section 5.3.1, and closed-loop stability of the nonlinear system is discussed in section 5.3.2.

5.1 Linearization, Time and Frequency domain representation

State space representation of the well model is presented in section 5.1.1. Further, the state space model is discretized in section 5.1.2 and a transfer function representation of the well model is derived in section 5.1.3.

5.1.1 State space representation

The part of the simulation model that represent the individual wells given by (3.34) - (3.36) is represented in state space using the following state and input vectors

$$\begin{aligned}\mathbf{x} &= \begin{bmatrix} p_{FBHP} & p_c^{in} & \overline{q} \end{bmatrix}^\top \\ &= \begin{bmatrix} x_1 & x_2 & x_3 \end{bmatrix}^\top \\ \mathbf{u} &= \begin{bmatrix} f & G_c(z_c) \end{bmatrix} \\ &= \begin{bmatrix} u_1 & u_2 \end{bmatrix}\end{aligned}$$

The nonlinear state space model is given according to

$$\begin{aligned}\dot{\mathbf{x}} &= \begin{bmatrix} \frac{\beta_1}{V_1}\left(PI\left(p_r - x_1\right) - x_3\right) \\ \frac{\beta_2}{V_2}\left(x_3 - k\sqrt{x_2 - p_{man}}u_2\right) \\ \frac{\overline{A}}{\overline{\rho l}}\Big(x_1 - x_2 + \Delta p_{ESP}(u_1) - \frac{\left(B_0^1+B_1^1\right)}{A_1}\frac{\rho_1}{2}x_3^2 - \frac{\left(B_0^2+B_1^2\right)}{A_2}\frac{\rho_2}{2}x_3^2 \\ \qquad -\rho_1 g(h_r - h_p) - \rho_2 g(h_p - h_c)\Big) \end{bmatrix} \\ &= \begin{bmatrix} f_1(\mathbf{x}) \\ f_2(\mathbf{x},\mathbf{u}) \\ f_3(\mathbf{x},\mathbf{u}) \end{bmatrix} \qquad (5.1) \\ y &= p_p^{in} \\ &= x_2 + \frac{\left(B_0^2 + B_1^2\right)}{A_2}\frac{\rho_2}{2}x_3^2 + \rho_2 g\left(h_p - h_c\right) - \Delta p_{ESP}(u_1) \\ &= h(\mathbf{x},\mathbf{u}) \qquad (5.2)\end{aligned}$$

where the ESP intake pressure are used as output from the system.

5.1.2 Linearization

The nonlinear state space model from (5.1) - (5.2) is linearized about an equilibrium state $\mathbf{x}^{eq}$ and input $\mathbf{u}^{eq}$ using Chen [1999, Eq. (2.21)]

$$\begin{aligned}\dot{\overline{\mathbf{x}}} &= \left[\begin{array}{ccc} \frac{\delta f_1}{\delta x_1} & \frac{\delta f_1}{\delta x_2} & \frac{\delta f_1}{\delta x_3} \\ \frac{\delta f_2}{\delta x_1} & \frac{\delta f_2}{\delta x_2} & \frac{\delta f_2}{\delta x_3} \\ \frac{\delta f_3}{\delta x_1} & \frac{\delta f_3}{\delta x_2} & \frac{\delta f_3}{\delta x_3} \end{array}\right]\Bigg|_{(\mathbf{x},\mathbf{u})=(\mathbf{x}_{eq},\mathbf{u}_{eq})} \overline{\mathbf{x}} + \left[\begin{array}{cc} \frac{\delta f_1}{\delta u_1} & \frac{\delta f_1}{\delta u_1} \\ \frac{\delta f_2}{\delta u_1} & \frac{\delta f_2}{\delta u_2} \\ \frac{\delta f_3}{\delta u_1} & \frac{\delta f_3}{\delta u_2} \end{array}\right]\Bigg|_{(\mathbf{x},\mathbf{u})=(\mathbf{x}_{eq},\mathbf{u}_{eq})} \overline{\mathbf{u}} \\ \overline{y} &= \left[\begin{array}{ccc} \frac{\delta h}{\delta x_1} & \frac{\delta h}{\delta x_2} & \frac{\delta h}{\delta x_3} \end{array}\right]\Bigg|_{(\mathbf{x},\mathbf{u})=(\mathbf{x}_{eq},\mathbf{u}_{eq})} \overline{\mathbf{x}} + \left[\begin{array}{cc} \frac{\delta h}{\delta u_1} & \frac{\delta h}{\delta u_2} \end{array}\right]\Bigg|_{(\mathbf{x},\mathbf{u})=(\mathbf{x}_{eq},\mathbf{u}_{eq})} \overline{\mathbf{u}}\end{aligned}$$

where $\overline{\mathbf{x}} = \mathbf{x}_{eq} - \mathbf{x}$ and $\overline{\mathbf{u}} = \mathbf{u}_{eq} - \mathbf{u}$ are deviation variables. Inserting the partial derivatives of f_1, f_2, f_3 and h, the following linearized state space model is obtained

$$\begin{aligned}
\dot{\overline{\mathbf{x}}} &= \begin{bmatrix} -\frac{\beta_1 PI}{V_1} & 0 & -\frac{\beta_1}{V1} \\ 0 & -\frac{1}{2}\frac{\beta_2}{V_2} k \left(x_2^{eq} - p_{man}\right)^{-1/2} u_2^{eq} & \frac{\beta_2}{V_2} \\ \frac{\overline{A}}{\overline{\rho} l} & -\frac{\overline{A}}{\overline{\rho} l} & -\left(\frac{\left(B_0^1+B_1^1\right)\rho_1}{A_1} + \frac{\left(B_0^2+B_1^2\right)\rho_2}{A_2}\right) x_3^{eq} \end{bmatrix} \overline{\mathbf{x}} \\
&\quad + \begin{bmatrix} 0 & 0 \\ 0 & \frac{\beta_2}{V_2} k \sqrt{x_2^{eq} - p_{man}} \\ \frac{2\overline{A}}{\overline{\rho} l} \frac{\rho_2 g}{f_0^2} H_0 u_1^{eq} & 0 \end{bmatrix} \overline{\mathbf{u}} \\
&= \begin{bmatrix} -a_{11} & 0 & -a_{13} \\ 0 & -a_{22} & a_{23} \\ a_{31} & -a_{32} & -a_{33} \end{bmatrix} \overline{\mathbf{x}} + \begin{bmatrix} 0 & 0 \\ 0 & b_{22} \\ b_{31} & 0 \end{bmatrix} \overline{\mathbf{u}} \qquad (5.3) \\
&= \mathbf{A}\overline{\mathbf{x}} + \mathbf{B}\overline{\mathbf{u}}
\end{aligned}$$

$$\begin{aligned}
\overline{y} &= \begin{bmatrix} 0 & 1 & \frac{\left(B_0^2+B_1^2\right)}{A_2}\rho_2 \end{bmatrix} \overline{\mathbf{x}} + \begin{bmatrix} 2\frac{\rho_1 g H_0}{f_0^2} & 0 \end{bmatrix} \overline{\mathbf{u}} \\
&= \begin{bmatrix} 0 & c_{12} & c_{13} \end{bmatrix} \overline{\mathbf{x}} + \begin{bmatrix} d_{12} & 0 \end{bmatrix} \overline{\mathbf{u}} \qquad (5.4) \\
&= \mathbf{C}^\top \overline{\mathbf{x}} + \mathbf{D}^\top \overline{\mathbf{u}}
\end{aligned}$$

An underlying assumption in the deduction above is that the ESP provide constant head H_0 about the equilibrium point $(\mathbf{x}_{eq}, \mathbf{u}_{eq})$ such that

$$\Delta p_{ESP}(u_1) \approx \rho_2 g H_0 \frac{u_1^2}{f_0^2}$$

By introducing the requirements

$$\begin{aligned}
x_2^{eq} - p_{man} &> 0 \qquad (5.5) \\
H_0 &> 0 \qquad (5.6) \\
u_1^{eq}, u_2^{eq}, x_3^{eq} &> 0 \qquad (5.7)
\end{aligned}$$

one can easily verify that

$$\begin{aligned}
a_{11} &= \frac{\beta_1 PI}{V_1} && > 0\\
a_{13} &= \frac{\beta_1}{V1} && > 0\\
a_{22} &= \frac{1}{2}\frac{\beta_2}{V_2} k \left(x_2^{eq} - p_{man}\right)^{-1/2} u_2^{eq} && > 0\\
a_{23} &= \frac{\beta_2}{V_2} && > 0\\
a_{31} &= \frac{\bar{A}}{\bar{\rho}\bar{l}} && > 0\\
a_{32} &= \frac{\bar{A}}{\bar{\rho}\bar{l}} && > 0\\
a_{33} &= \left(\frac{\left(B_0^1+B_1^1\right)\rho_1}{A_1} + \frac{\left(B_0^2+B_1^2\right)\rho_2}{A_2}\right) x_3^{eq} && > 0\\
b_{22} &= \frac{\beta_2}{V_2} k \sqrt{x_2^{eq} - p_{man}} && > 0\\
b_{31} &= \frac{2\bar{A}}{\bar{\rho}\bar{l}} \frac{\rho_2 g}{f_0^2} H_0 u_1^{eq} && > 0\\
c_{12} &= 1 && > 0\\
c_{13} &= \frac{\left(B_0^1+B_1^1\right)\rho_1}{A_1} x_3^{eq} && > 0
\end{aligned}$$

if all the remaining system parameters are positive.

5.1.3 Transfer function representation

The transfer function representation of a linear state space model is given by Chen [1999, Eq. (2.16)] according to

$$\begin{aligned}
\frac{Y}{U}(s) &= \mathbf{C}^\top \left(s\mathbf{I} - \mathbf{A}\right)^{-1} \mathbf{B} + \mathbf{D}^\top\\
&= \mathbf{G}(s)
\end{aligned}$$

By inserting the matrices from (5.3) - (5.4) the following transfer functions are obtained

$$\begin{aligned}
\mathbf{G}(s) &= \left[\begin{array}{c} \frac{d_{12}n_3 s^3 + (d_{12}n_2 - b_{31}c_{13})s^2 + (d_{12}n_1 + b_{31}(a_{31} - (a_{11}+a_{22})c_{13}))s + d_{12}n_0 + a_{22}b_{31}(a_{31} - a_{11}c_{13})}{n_3 s^3 + n_2 s^2 + n_1 s + n_0} \\ \frac{-a_{23}b_{22}c_{13}s + a_{23}b_{22}(a_{31} - a_{11}c_{13})}{n_3 s^3 + n_2 s^2 + n_1 s + n_0} \end{array}\right]\\
&= \left[\begin{array}{cc} G_1(s) & G_2(s) \end{array}\right] \qquad (5.8)
\end{aligned}$$

where the denominator coefficients are

$$\begin{aligned}
n_3 &= 1\\
n_2 &= a_{11} + a_{22} + a_{33}\\
n_1 &= a_{11}a_{22} + a_{11}a_{33} + a_{22}a_{33} + a_{23}a_{32} + a_{13}a_{31}\\
n_0 &= a_{11}a_{22}a_{33} + a_{11}a_{23}a_{32} + a_{13}a_{22}a_{31}
\end{aligned}$$

The deduction of $\mathbf{G}(s)$ is quite extensive and of minor importance in the analysis. Thus, the complete deduction is presented in appendix B.1.

5.2 Open-loop stability

Provided that the limitations given by (5.5) - (5.7) are met, the deduction in section 5.2.1 prove that the linearized system is asymptotically stable about any equilibrium point. Further, the proof of asymptotic stability of the linearized system is used to conclude on open-loop stability of the nonlinear system in section 5.2.2.

5.2.1 Linearized system

Asymptotic stability of a linear system is investigated by evaluating the roots of the system. The roots appear as zeros in the characteristic polynomial

$$\lambda(s) = |s\mathbf{I} - \mathbf{A}|$$

By inserting the system matrix from (5.3) and solving for the matrix determinant the following polynomial is obtained

$$\begin{aligned}
\lambda(s) &= \begin{vmatrix} s+a_{11} & 0 & a_{13} \\ 0 & s+a_{22} & -a_{23} \\ -a_{31} & a_{32} & s+a_{33} \end{vmatrix} \\
&= (s+a_{11})\left((s+a_{22})(s+a_{33}) - (-a_{23})a_{32}\right) + a_{13}\left(-(s+a_{22})(-a_{31})\right) \\
&= s^3 + (a_{11}+a_{22}+a_{33})s^2 + (a_{22}a_{33}+a_{13}a_{31})s + a_{11}a_{22}a_{33} + a_{13}a_{22}a_{31} \\
&= \lambda_3 s^3 + \lambda_2 s^2 + \lambda_1 s + \lambda_0
\end{aligned}$$

where

$$\begin{aligned}
\lambda_3 &= 1 \\
\lambda_2 &= a_{11}+a_{22}+a_{33} \\
\lambda_1 &= a_{22}a_{33}+a_{13}a_{31} \\
\lambda_0 &= a_{11}a_{22}a_{33}+a_{13}a_{22}a_{31}
\end{aligned}$$

Then, according to Routh's criterion presented in Balchen et al. [2004, p. 260] the four elements in the leftmost column in the Routh's table needs to have the same sign if all the zeros of the polynomial is to lie in the open left half plane. The Routh's table are given according to

λ_3	λ_1
λ_2	λ_0
β_2	β_2
ζ_2	

where

$$\begin{aligned}
\beta_2 &= \frac{-\begin{vmatrix} \lambda_3 & \lambda_1 \\ \lambda_2 & \lambda_0 \end{vmatrix}}{\lambda_2} = \frac{\lambda_1\lambda_2 - \lambda_0\lambda_3}{\lambda_2} \\
\beta_0 &= \frac{-\begin{vmatrix} \lambda_3 & 0 \\ \lambda_2 & 0 \end{vmatrix}}{\lambda_2} = \frac{0\cdot\lambda_2 - 0\cdot\lambda_3}{\lambda_2} = 0 \\
\zeta_2 &= \frac{-\begin{vmatrix} \lambda_2 & \lambda_1 \\ \beta_2 & \beta_0 \end{vmatrix}}{\lambda_2} = \frac{\lambda_1\cdot\beta_2 - \lambda_2\cdot\beta_0}{\lambda_2} \\
&= \frac{\lambda_1(\lambda_1\lambda_2 - \lambda_0\lambda_3)}{\lambda_2^2}
\end{aligned}$$

Inserting β_1, β_2 and ζ_2 in Routh's table yield

λ_3	λ_1
λ_2	λ_0
$\frac{\lambda_1\lambda_2-\lambda_0\lambda_3}{\lambda_2}$	0
$\frac{\lambda_1(\lambda_1\lambda_2-\lambda_0\lambda_3)}{\lambda_2^2}$	

Since $\lambda_2, \lambda_3 > 0$, every element in the leftmost column are positive if and only if

$$\lambda_1\lambda_2 - \lambda_0\lambda_3 > 0$$

By inserting for λ_i the condition is further developed according to

$$\begin{aligned}
&(a_{22}a_{33} + a_{13}a_{31})(a_{11} + a_{22} + a_{33}) \\
&\qquad -(a_{11}a_{22}a_{33} + a_{13}a_{22}a_{31})\cdot 1 > 0 \\
&\cancel{a_{11}a_{22}a_{33}} + a_{22}^2a_{33} + a_{22}a_{33}^2 + a_{11}a_{13}a_{31} + \cancel{a_{13}a_{22}a_{31}} \\
&\qquad +a_{13}a_{31}a_{33} - \cancel{a_{11}a_{22}a_{33}} - \cancel{a_{13}a_{22}a_{31}} > 0 \\
&\qquad a_{22}^2a_{33} + a_{22}a_{33}^2 + a_{11}a_{13}a_{31} + a_{13}a_{31}a_{33} > 0
\end{aligned}$$

Since $a_{i,j} > 0\ \forall(i,j)$ the condition holds and the system is asymptotically stable, i.e, the roots of the system are located in the open left half plane.

5.2.2 Nonlinear system

Since the linearized open-loop system is asymptotically stable the nonlinear open-loop is also asymptotically stable. This is given from theorem 4.7 in Chen [1999, p. 139].

5.3 Closed-loop stability

The system is set in closed-loop with the controller from section 4.4.3. Closed-loop stability of the linearized system from section 5.1.2 can easily be determined using frequency response analysis. Closed-loop stability is proven in section 5.3.1 using the Nyquist stability criteria. Closed-loop stability of the nonlinear system is discussed in section 5.3.2.

5.3.1 Linearized system

Closed-loop stability of the linearized system can be determined by evaluating the frequency response of $det\left(\mathbf{I}+\mathbf{L}(s)\right)$ in a Nyquist-diagram, where $\mathbf{L}(s)=\mathbf{K}(s)\mathbf{G}(s)$ is the loop transfer function. The MIMO Nyquist closed-loop stability criteria is given in Skogestad and Postlethwaite [2005, Theorem 4.9, p. 152]

Both control inputs are controlled using the same PI-control law given by (4.4) which has the transfer function representation given by

$$\mathbf{K}(s)=\begin{bmatrix} K_p\frac{1+\tau_i s}{\tau_i s} \\ K_p\frac{1+\tau_i s}{\tau_i s} \end{bmatrix}$$

where $K_p=0.16$ and $\tau_i=0.4$. The loop transfer functions are accordingly

$$\begin{aligned}\mathbf{L}(s) &= \mathbf{K}(s)\mathbf{G}(s) \\ &= \begin{bmatrix} K_p\frac{1+\tau_i s}{\tau_i s} \\ K_p\frac{1+\tau_i s}{\tau_i s} \end{bmatrix} \cdot \\ &\quad \begin{bmatrix} \frac{d_{12}n_3s^3+(d_{12}n_2-b_{31}c_{13})s^2+(d_{12}n_1+b_{31}(a_{31}-(a_{11}+a_{22})c_{13}))s+d_{12}n_0+a_{22}b_{31}(a_{31}-a_{11}c_{13})}{n_3s^3+n_2s^2+n_1s+n_0} \\ \frac{-a_{23}b_{22}c_{13}s+a_{23}b_{22}(a_{31}-a_{11}c_{13})}{n_3s^3+n_2s^2+n_1s+n_0} \end{bmatrix}\end{aligned} \tag{5.9}$$

The frequency response of $det\,(\mathbf{I}+\mathbf{L}(s))$ represented in a Nyquist-diagram can be found using the MATLAB® function `nyquist(sys)` according to

```
nyquist(det(eye(2)+L))
```

where `eye(2)` is a unit matrix of dimension 2×2 and `L` is the transfer function matrix given by (5.9). The Nyquist-diagram is shown in figure 5.1, with a close-up of the origin given in figure 5.2.

For a open-loop stable system the Nyquist stability theorem states that if the frequency response of $det\,(\mathbf{I}+\mathbf{L}(s))$ do not pass through, or encircle, the origin as s goes from $-j\infty$ to $+j\infty$, then the closed-loop system is stable. Figure 5.1 and 5.2 clearly show that the trajectory do not encircle the origin, and consequently, the closed-loop system is stable.

5.3.2 Nonlinear system

Proving closed-loop stability - with this particular controller - is not a trivial task due to the presence of *hard* nonlinearities which complicate use of Lyapunov theory. It is a fairly simple task to develop a nonlinear controller that ensure asymptotic, or even exponential, closed-loop stability if this is desired (appendix B.2).

Although it is possible to employ a control law that ensure closed-loop stability this may not be desirable from a control design perspective. The

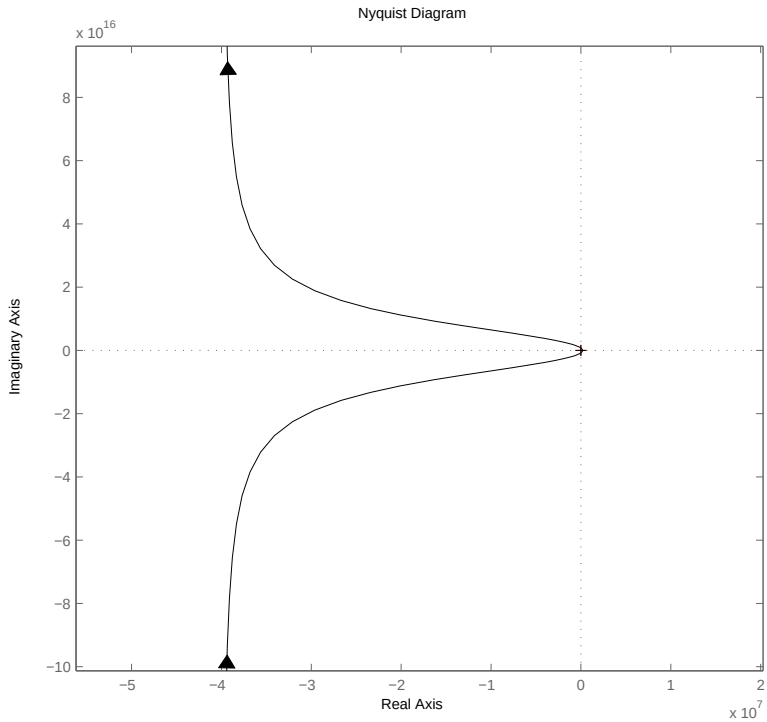

Figure 5.1: Nyquist plot of $det\left(\mathbf{I}+\mathbf{L}(s)\right)$

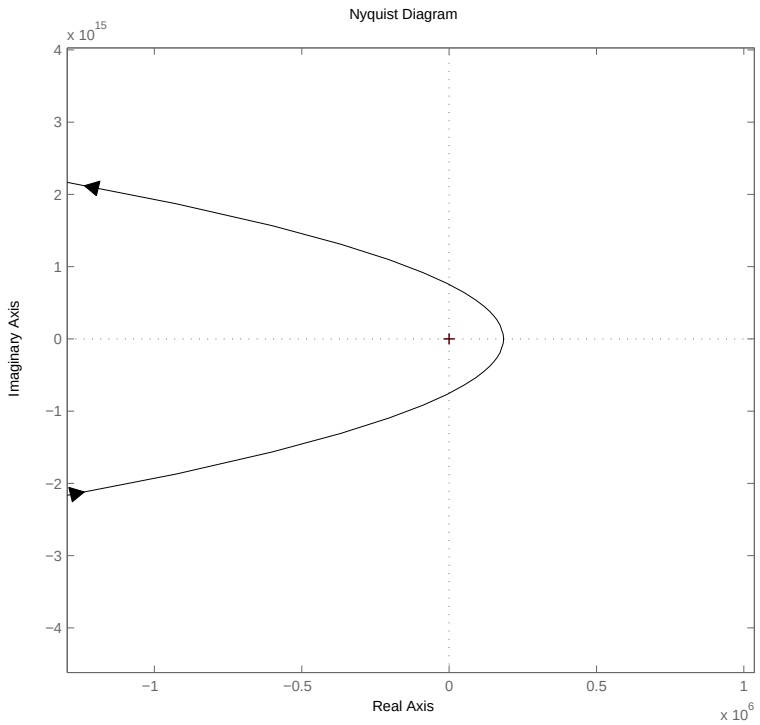

Figure 5.2: The Nyquist-plot does not encircle the origin and thereby proving closed-loop stability.

purpose of this thesis is to design a control system that satisfy certain requirements, and the complexity of this design problem grow with increased controller complexity.

Although it is difficult to prove closed-loop stability mathematically, there are certain features present in the system that support that this is in fact true. The presence of friction may signify that the system is passive and if this is the case, passivity theory can be used to conclude on stability of the closed-loop system. In this context a particularly useful deduction is presented in Egeland and Gravdahl [2003, Sec. 2.4.13], where it is stated that a feedback interconnection of passive systems are at least marginally stable.

Chapter 6

Simulation results

The simulation model from chapter3 is set in closed-loop with the control system presented in section 4.4 and simulated in MathWorks® MATLAB®. The closed-loop system is simulated on a range of different scenarios that is supposed to reflect real life situations which an ESP lifted well system may encounter. This chapter deals with the simulation of these scenarios and analysis of the results. Implementation aspects are treated in detail in appendix A.

Section 6.1 give a brief description of the different scenarios, and a description of how the simulation results are presented are provided in section 6.2. Each scenario is divided into a set of case study, where each case study deals with different aspects of the associated scenario. Simulations results obtained from the different case study is presented and analyzed in section 6.3 to 6.6. Finally, concluding remarks are given in section 6.7.

6.1 Scenario description

The scope of the different scenarios is to embrace a wide range of situations which may occur during normal operation of an ESP lifted well system. The following scenarios are included in the simulation study:

Step-change of set-point A basic event that the control system should be able to handle is a step-change in the pressure set-point. The control system should be able to track a step-change in set-point in one well, while maintaining a desired pressure set-points in the remaining wells. This scenario is treated in section 6.3.

Start-up/Shut-down of one well At some point in time during the life time of a well, various reasons may require a well to be shut-down or restarted. In this context, a well is considered to be shut-down when the ESP frequency is 0Hz with a choke position at 0%. The start-up phase is defined as the time taken from a start-up command is given until the ESP frequency reach 35Hz. Simultaneously, the choke opening is gradually increased to 20%. The well subject to start-up/shut-down conditions is allowed to violate its operational envelope, but the three remaining wells are required to comply with their respective envelopes. This scenario is treated in section 6.4.

ESP tripping An ESP unit is said to trip if something unexpected occurs which cause immediate pump failure. Pump failure is a serious event which significantly affects operation of the remaining wells in the system, and is perhaps one of the situations which demands most of the control system. This scenario is presented in section 6.5.

Start-up/Shut-down of booster-pump The way the booster-pump is operated greatly affect the flow rate from the manifold through the transportation line. By altering the operation frequency of the booster-pump, variations in flow occur which in turn causes variations in manifold and well pressure. The start-up sequence is regarded as the time taken from a start-up command is given until the operation frequency reaches 35Hz, and the shut-down sequence is defined as the time taken from the shut-down command is given until the frequency reaches 0Hz. This last scenario is dealt with in section 6.6.

6.2 Presentation of simulation results

The simulation model is comprised of four, mathematically identical wells. Since the four wells are identical, simulation data obtained from the different wells contain the same information if the wells are operated in an equal manner. In order to exclude redundant data, information collected from only two of the wells are included in the consecutive sections.

Information collected from simulations are presented in three figures; two of which display data related to the pressure control system in each well, and one that display the pressure profile and flow through the wells, the

manifold and transportation line. For simplicity, the two wells are denoted *Well 1* and *Well 2*.

6.3 Scenario I: Change of pressure set-point

There are several interesting angles to this scenario. In order to illustrate the complete functionality of the control system, an initial case study is performed where the ESP is operated within the operational envelope. This case study is presented in section 6.3.1. In section 6.3.2, a second case study is presented where the ESP is actively operated along the upthrust constraint. Active frequency limitations will appear in other scenarios and are thus not included as a stand-alone case.

6.3.1 Case I: Operation within the envelope

The ESP intake pressure set-point in Well 1 is stepped up from 30bar to 50bar after 20 seconds, as shown in figure 6.1. The control system is able to track the pressure set-point in a smooth manner, where the control error is completely eliminated after 18 seconds. By examining the trajectory of the control error it is clear that the selected controller parameters yield a good closed-loop response, i.e., with rapid convergence to $e = 0$ without oscillations. The control error trajectory suggests that the control system is critically damped. The control system acts by adjusting the ESP frequency from 53Hz to 42Hz while leaving the choke position unchanged at 100%.

Well 2 experience only a minute influence from the change of operation of Well 1. Well 2 is also operated within its operational envelope and the control system is able keep the control error at an adequate level, as seen from figure 6.2. The reader might notice that the control system use approximately 180 seconds to completely remove the control error and this may be interpreted as an indication that the integral time in the controller is too low. However, by keeping in mind that the maximum control error in this instance is below 0.3% it is the writer's opinion that insignificant performance improvement can be attained by further tuning the control system.

Change in pressure profile in Well 1 from the changed ESP intake pressure cause effects that propagate throughout the system and effect the pressure profile and flow through the manifold and the remaining wells. This effect is shown in figure 6.3. From the upper, rightmost subfigure it is clear that

the control of the ESP intake pressure enables accurate control of the flow through the well, and that an increase in ESP pressure cause a decrease in flow.

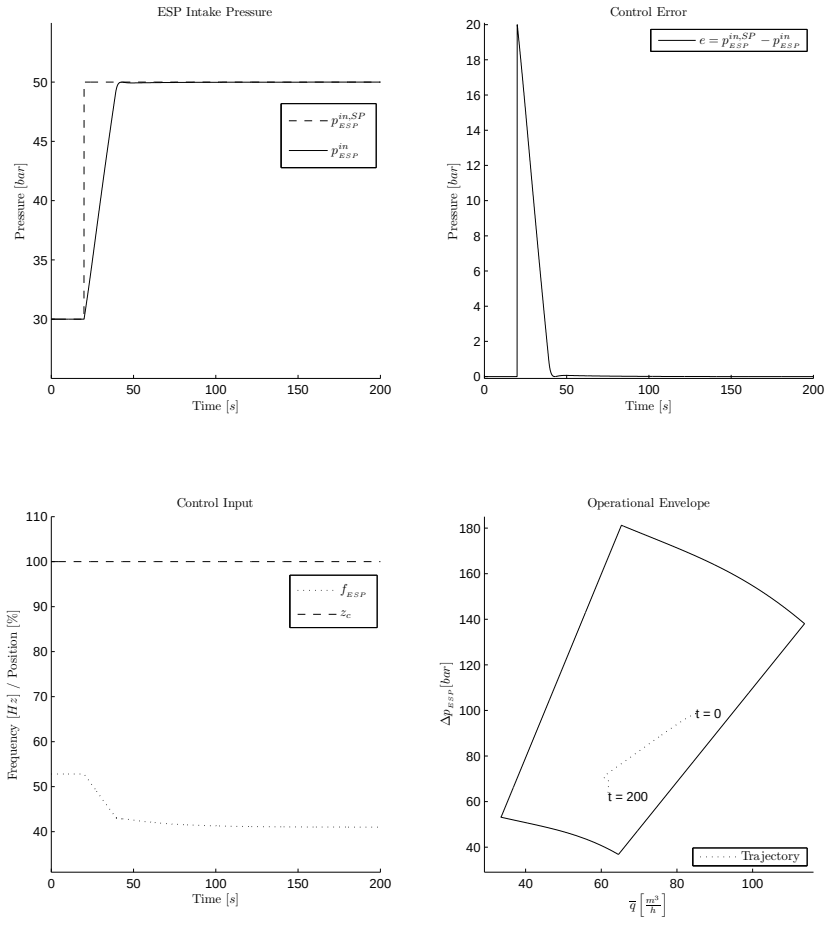

Figure 6.1: A step-change in ESP intake pressure set-point in Well1 cause a change in the primary control input f_{ESP}. The $\overline{q} - \Delta p_{ESP}$ trajectory show that the ESP is operated within the operational envelope.

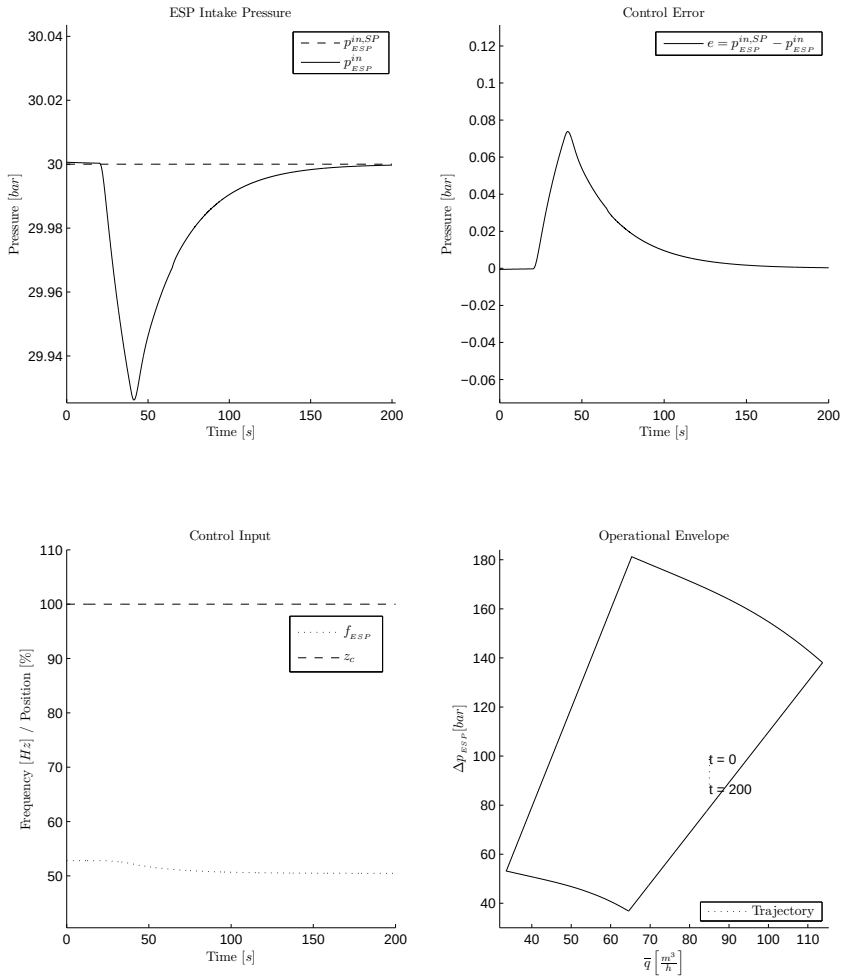

Figure 6.2: Well2 experience only minor influence from a change of ESP intake pressure set-point in Well1. Well2 is operated within the envelope and the control system is able to eliminate the control error.

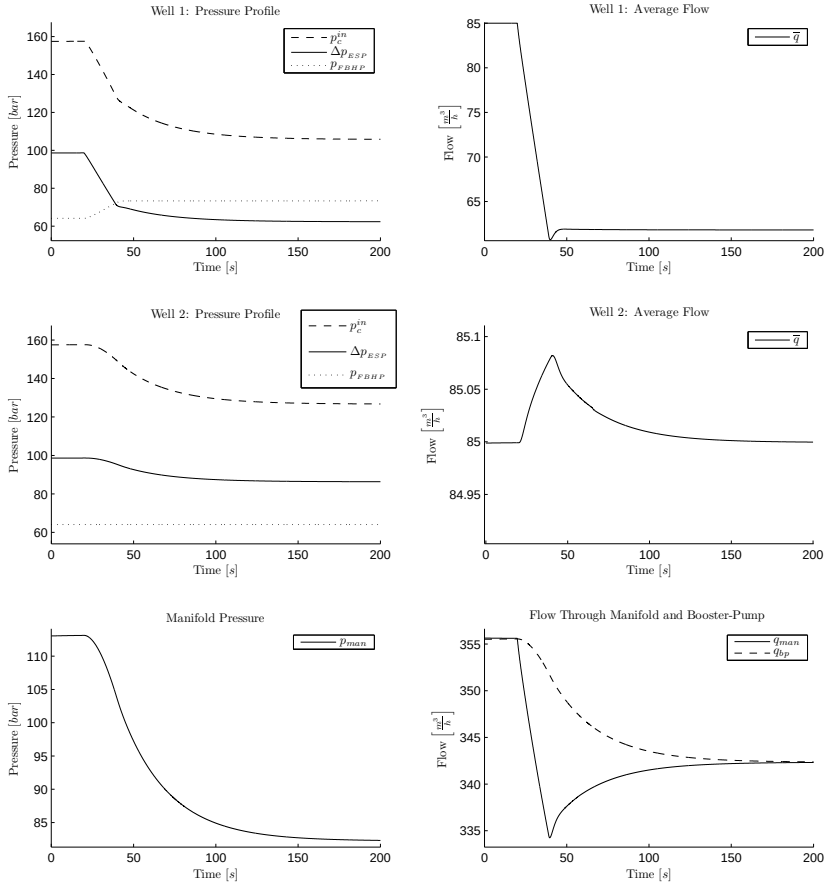

Figure 6.3: The flow through Well1 is highly dependant of the ESP intake pressure. This support the statement made by Takacs [2009], that the flow through an ESP lifted well is best controlled by controlling the ESP intake pressure.

6.3.2 Case II: Operation with active upthrust constraint

In this situation a step-change in ESP intake pressure set-point is imposed in the opposite direction from the previous case. After 20 seconds the pressure set-point in Well 1 is changed from 30bar to 5bar, as displayed in figure 6.4.

The control system is in this instance subject to different challenges than in the previous case. The close-up subfigure of the ESP operational envelope show that the ESP is operated close to its upthrust constraint prior to the change in ESP intake pressure set-point, and that the control system cause the ESP to traverse the upthrust constraint during the active control period. As the ESP traverse the upthrust constraint the control system require use of both the ESP frequency and choke position as control inputs. This coincides with the control system requirement that the choke position is only to be used in situations where use of only the ESP frequency as control input is inadequate.

Another interesting observation can be made from examining the trajectory in the ESP operational envelope. As the trajectory leaves the upthrust constraint after 75 seconds, the control system has brought the well into a state where the use of the choke position as control input is no longer necessary. At this point in time the choke position is 95% and the ESP frequency is 62.5Hz. In the subsequent time interval, the control system continuously reallocates the inputs until it derives at a combination where the choke position is as high as possible (without implicating addition control error). In this instance, the best combination of control inputs is with a choke position of 100% and an ESP frequency of 64Hz.

Since the control system use the secondary control input actively to eliminate the control error, the convergence rate of the control error is lower than in the previous case. This is explained from more restrictive rate limitations on the choke input than the ESP frequency. As a comparison, the control system use 60 seconds to eliminate the control error in this instance while it spent 18 seconds in the previous case.

Figure 6.5 show that Well 2 only experience a minor influence from the change in ESP intake pressure set-point in Well 1. The behavior of Well 2 is similar to the behavior observed in the previous case, but the maximum control error is slightly less in this instance. The control system in Well 2 has no difficulty in maintaining the desired ESP intake pressure.

By reducing the ESP intake pressure in Well 1, the flow through the well increases. The overall effect from an increase in flow from Well 1 is

increased manifold flow and pressure, as seen from figure 6.6. The flow through Well 2 is slightly decreased in a short period before the control system is able to restore desired ESP intake pressure, after which the original flow is restored.

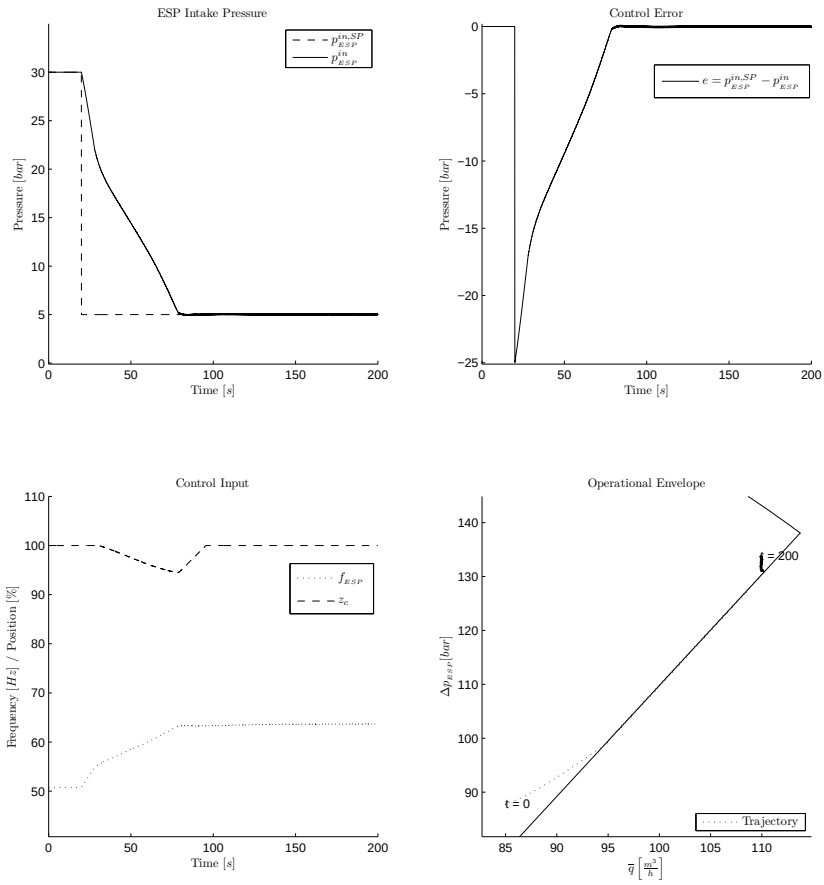

Figure 6.4: A step-change in the ESP intake pressure set-point in Well1 imply that the ESP unit is operated along the upthrust constraint. Both control inputs are needed in order to keep the ESP unit operated within the operational envelope and to eliminate the control error.

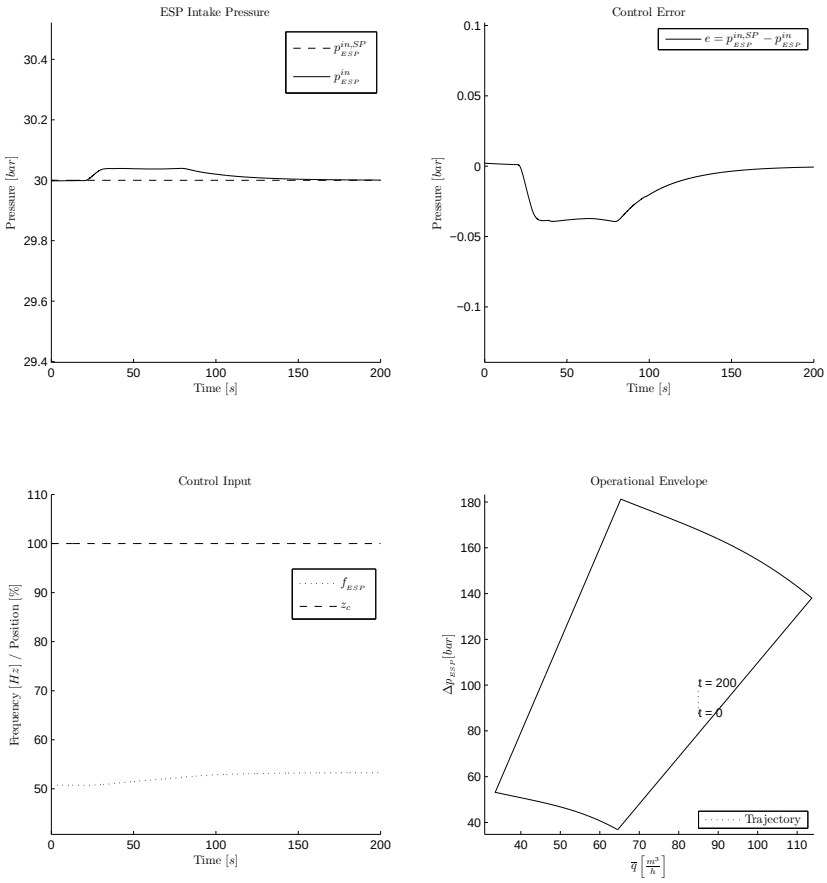

Figure 6.5: The control system in Well2 is able to maintain a fairly constant ESP intake pressure.

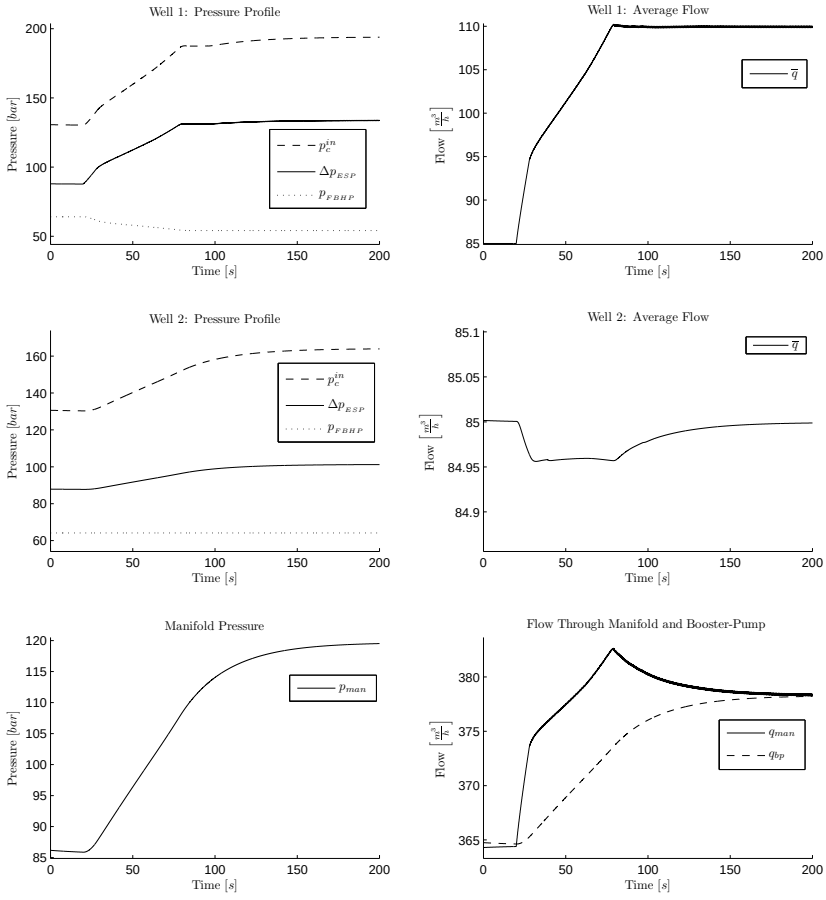

Figure 6.6: By decreasing the ESP intake pressure in Well 1, the flow through the well is increased substantially.

6.4 Scenario II: Start-up/Shut-down of one well

Some situations may require a well to temporary shut-down and restarted. These scenarios are interesting from a control point of view since they involve violation of the operational envelope, and it is important that the control system is able handle these situations in an efficient manner. The start-up scenario is treated in section 6.4.1, where the Well 1 is initially shut-down before a restart command is given. Section 6.4.2 deals with the opposite case where Well 1 is subject to shut-down during normal operation.

6.4.1 Case I: Well start-up

In this situation Well 1 is initially shut-down before a start-up command is given after 20 seconds of simulation. The start-up sequence involve that the ESP frequency is ramped up from 1Hz to 35Hz at a rate of 10Hz/s. As the pressure builds up in the well and becomes larger than the manifold pressure the choke opening is gradually increased from 0% to 20% at a rate of 1/3 percent per second. The pressure controller is deactivated during the start-up phase and is activated when the ESP frequency reach 35Hz.

Figure 6.7 provide a clear overview of a well start-up procedure. The frequency rate of 10 Hz/s brings the ESP frequency up to 35Hz in a matter of seconds. The steep rate of change in frequency creates a pressure impulse that propagates throughout the well and the rest of the system. The pressure impulse causes the trajectory in the q-dp diagram to behave in an irregular manner. The trajectory starts at the origin and rapidly advances up to the borderline of the operational envelope, but at this point in time there is a flow impulse present in the well (as seen from figure 6.9). As the pressure and flow impulses rapidly die out, the trajectory move from the borderline of the operational envelope and down to the encircled point in the diagram. The behavior during this phase is independent of the pressure control system.

The control system is activated after the start-up phase is completed. The control system brings the operation of the ESP unit back inside the operational envelope by increasing the choke position. During the time from the start-up is completed until approximately 320 seconds into simulation, the control system is able to keep the ESP unit operated within the envelope and continuously reallocates use of input until it arrives at the combination where the choke position is as high as possible. The reader might notice that the control error is eliminated after just 190 seconds

of simulations, while the reallocation of inputs takes an additional 130 seconds.

Figure 6.8 display how Well 2 is influenced from the start-up of Well 1. An interesting remark in this respect is that Well 2 is operated in active upthrust before Well 1 is started up, with an ESP frequency of 42Hz and a choke position of 89 percent. The ESP unit in Well 2 is in this case operated in a suboptimal manner from an input point of view, since the choke position is less than 100%. After Well 1 is started up the changed manifold pressure enables Well 2 to be operated in a different manner, with a different combination of control inputs. The result from the start-up procedure in Well 1 is that Well 2 is operated from a more optimal manner (again, from an input point of view). It is clear from figure 6.8 that the pressure control system in Well 2 has little difficulty in keeping the ESP unit operated within the operational envelope during the start-up of Well 2.

The start-up of Well 1 has great impact on the pressure profile in both wells and the manifold, as seen from figure 6.9. The previously mentioned flow impulse in Well 1 is seen in the upper right subfigure propagate through the manifold and, in turn, influence the flow through Well 2. The flow impulse dies out quite rapidly and the different flows in the system return to their normal values.

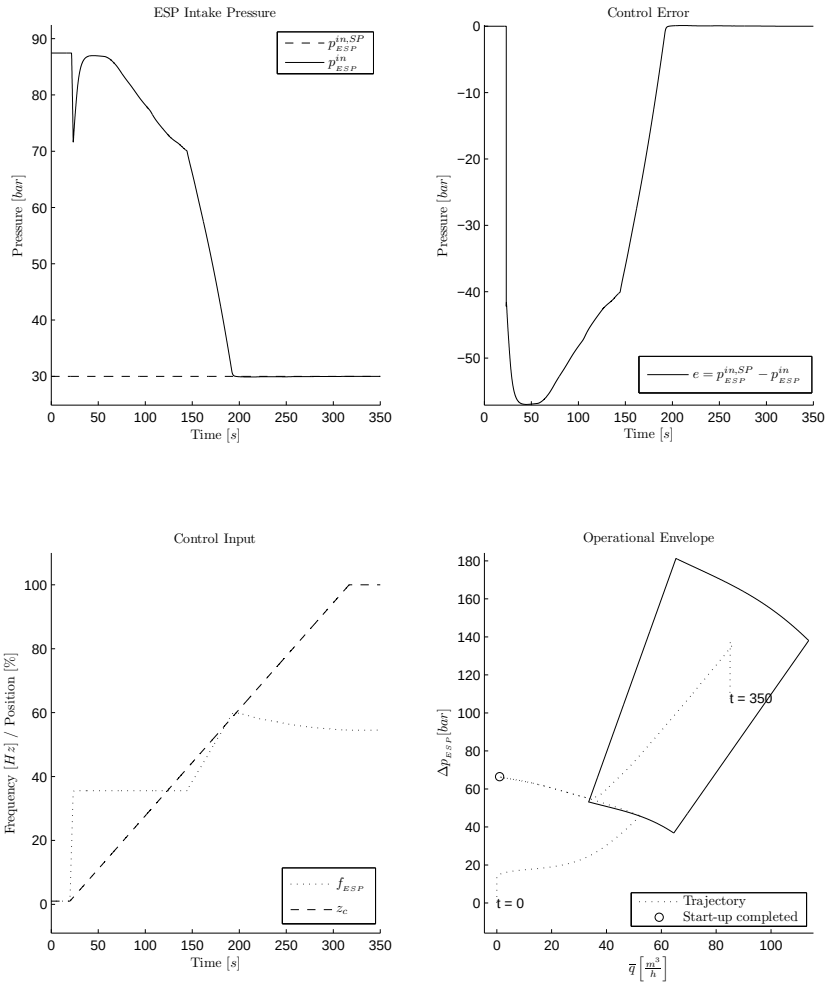

Figure 6.7: The large rate of change in ESP frequency cause a pressure and flow impulse in the system.

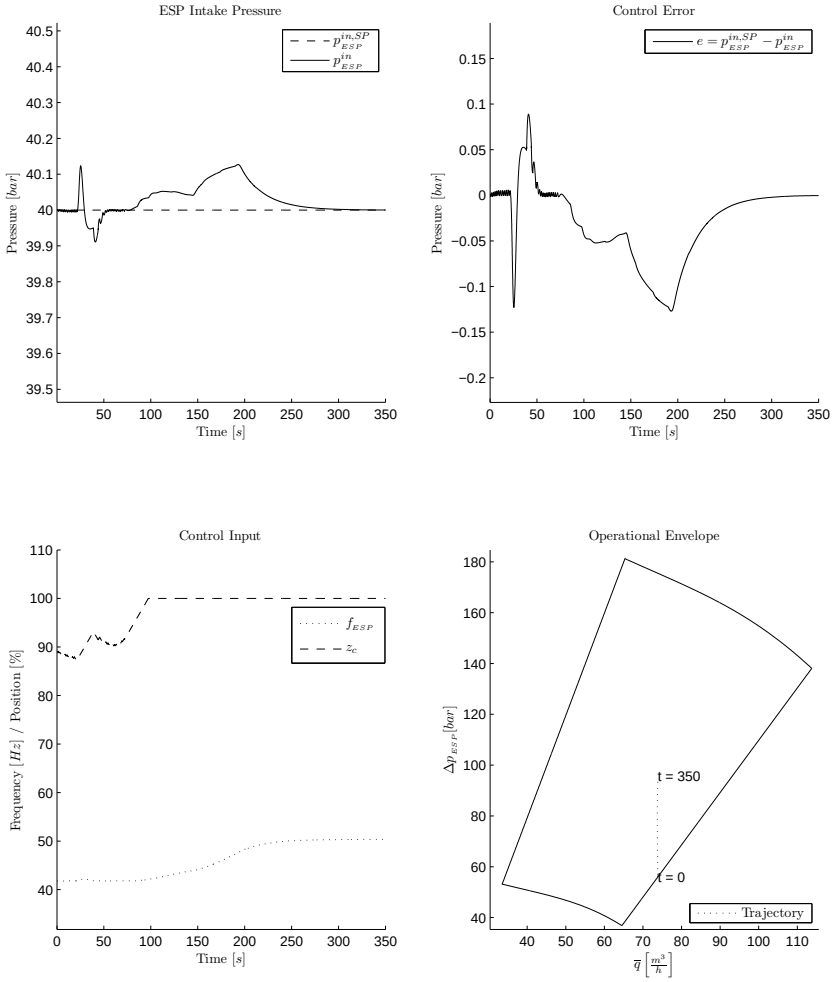

Figure 6.8: The pressure and flow impulse cause irregular behavior in Well 2.

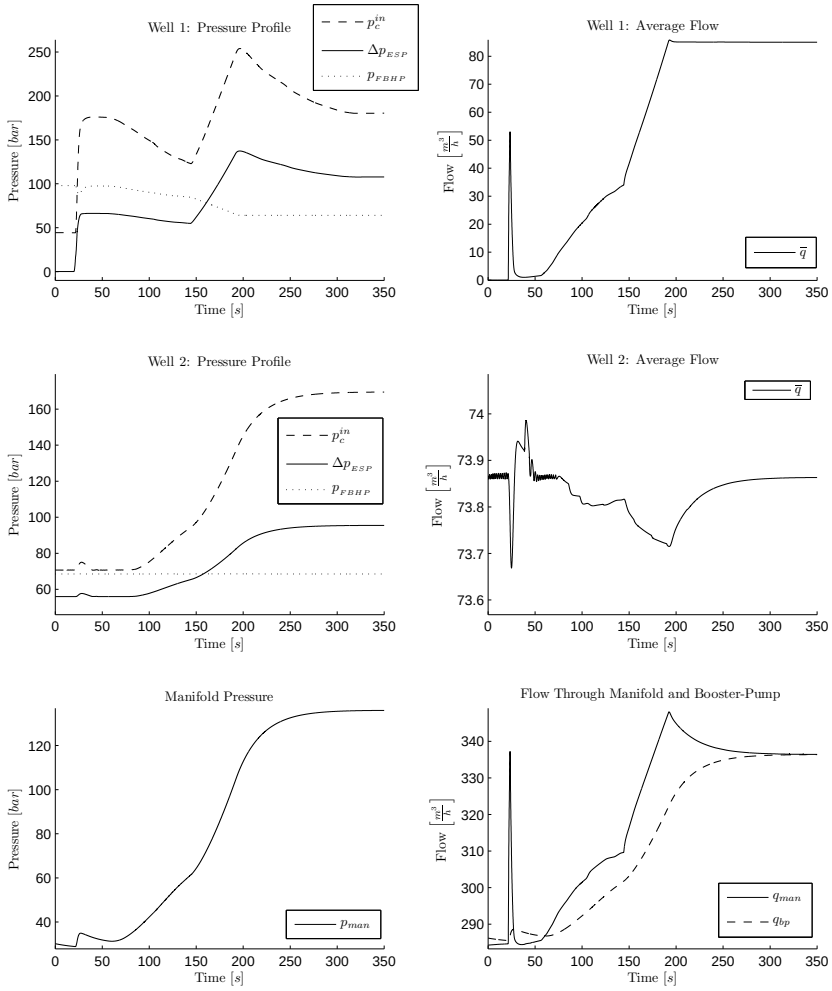

Figure 6.9: The start-up sequence cause large changes in the pressure profiles in both wells and the manifold.

6.4.2 Case II: Well shut-down

In this situation both the ESP units in both wells are initially operated within the operational envelope. Then, after 20 seconds of simulation a shut-down command is given to Well 1 which enforce a shut-down of the ESP unit and closing of the wellhead choke. In this respect, the shut-down sequence involves setting the ESP frequency to 1Hz and the choke opening to one percent. The original frequency and choke position rate limitations are uphold during the shut-down phase.

Figure 6.10 display the behavior of Well 1 during the shut-down phase. The subfigure representing the control error is of little interest since the pressure control system is deactivated during this phase. The shut-down procedure is quite time extensive due to the strict rate limitations, Well 1 use approximately 300 seconds to complete the shut-down sequence.

Due to the long duration of the shut-down sequence the changes occurring in Well 1 are slow varying compared to the other cases. Slow varying changes in Well 1 cause slow varying changes in the manifold pressure and, in turn, slow varying changes in Well 2. From a control perspective this is good news since slow varying changes are easier to handle than fast varying changes. This fact is evident by examining the control error in figure 6.11, where a maximum control error of less than 0.4% is observed. Also, figure 6.11 clearly show that the control system is capable of keeping the ESP unit in Well 2 operated within the operational envelope during the shut-down sequence of Well 2.

There is little new information contained in figure 6.12 besides noting that the behavior of the pressure in both wells and the manifold during the shut-down sequence are more smooth and regular than during the start-up sequence. Naturally, the flow from the manifold through transportation line is reduced since the production rate in Well 1 comes to a halt.

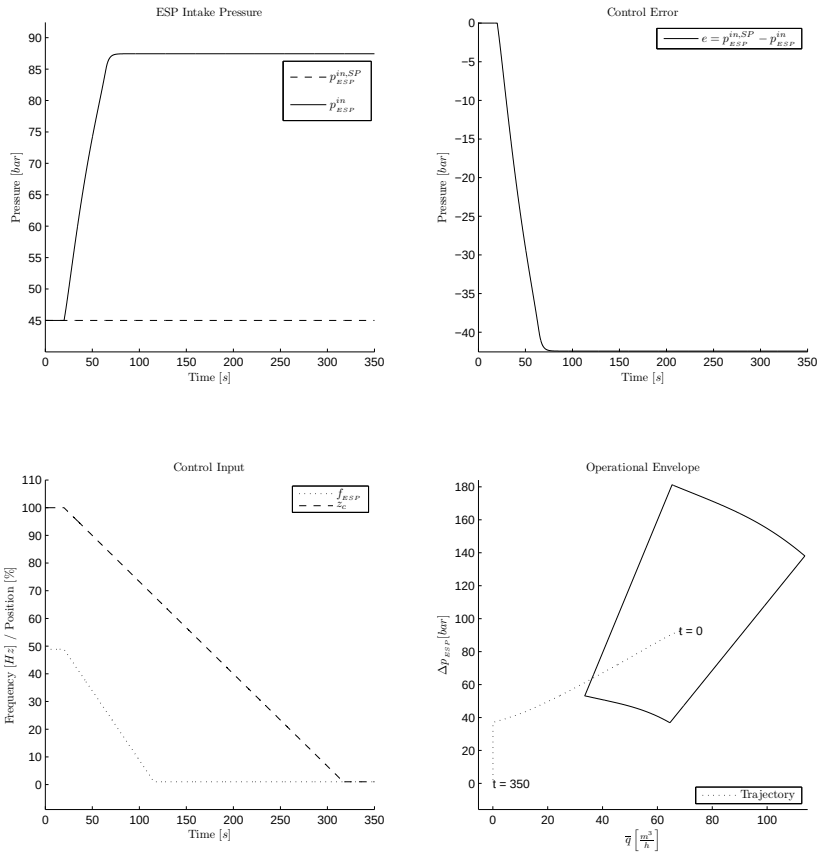

Figure 6.10: The control system in Well 1 is diabled during the shut-down sequence and thus, the control error is of little interest in this case.

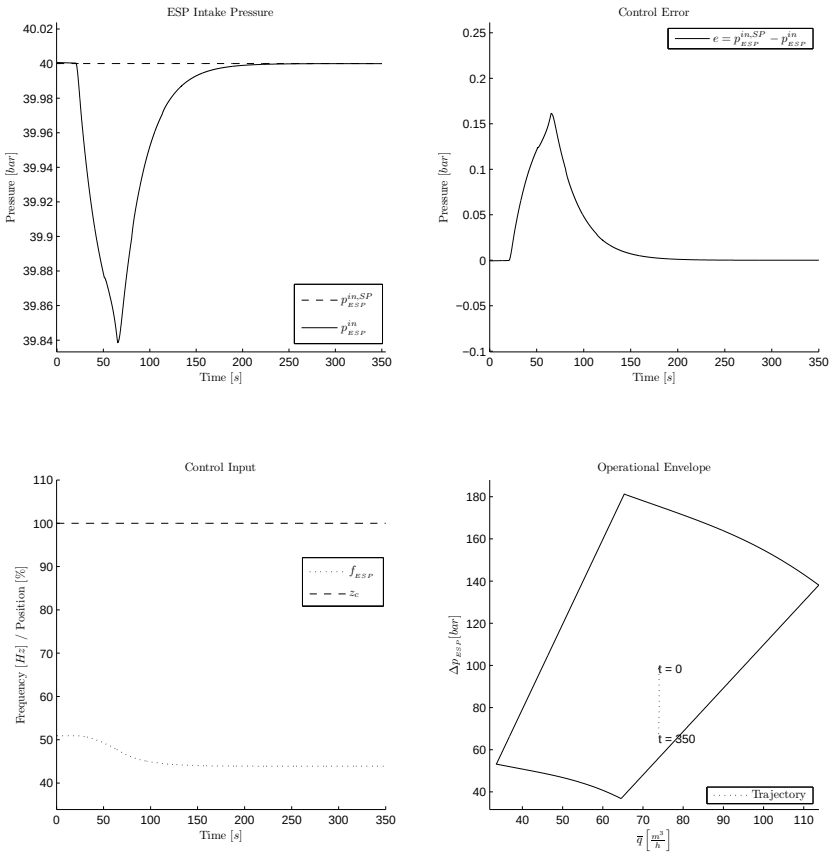

Figure 6.11: The shut-down procedure cause more smooth behavior in Well 2 due to strict frequency rate limitations in Well 1.

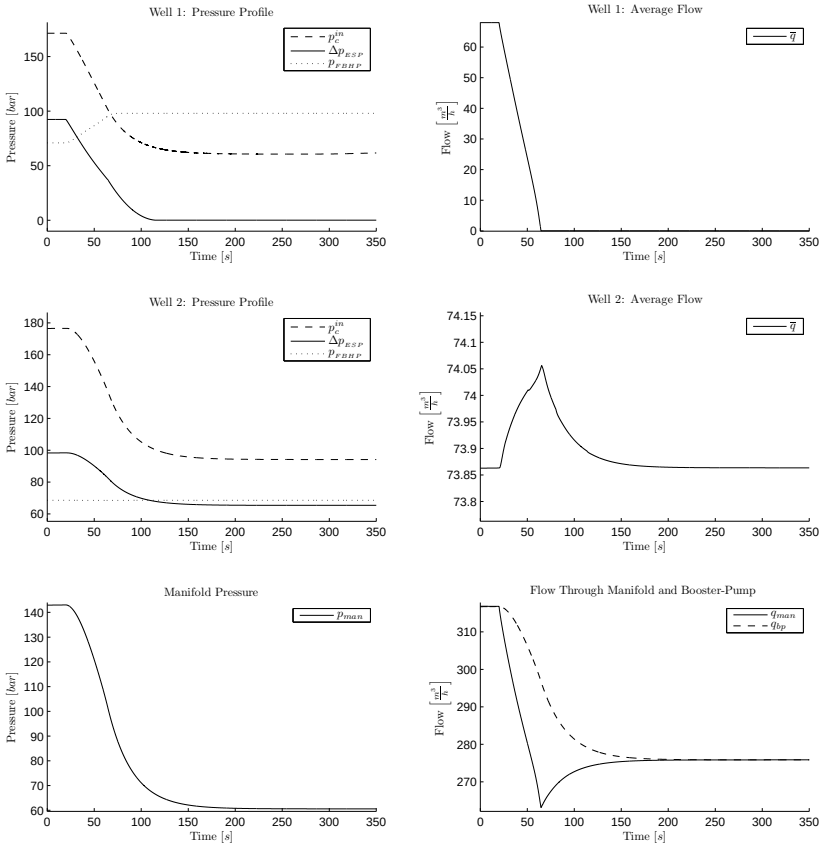

Figure 6.12: The shut-down sequence lead to a complete stop in production from Well 1, naturally, and a reduced flow from the manifold through the transportation line.

6.5 Scenario III: ESP tripping

When an ESP unit trips, an unexpected event cause a sudden drop in ESP frequency which renders the unit ineffective. In this context, the trip sequence cause the ESP frequency to drop down to 1Hz at a rate of 20Hz/s while the choke position in the respective well is left unchanged. The control system is deactivated as the trip sequence is initiated. Also, in this case the ESP frequency is not allowed to become less than 1Hz in order to avoid any numerical issues during simulation.

The following section presents a case study where the ESP unit in Well 1 trips.

6.5.1 Case I: ESP tripping in Well 1

The ESP unit in Well 1 is given the command to trip after 20 seconds of simulation. The trip command initiate the trip sequence described in the previous paragraph and accordingly, the ESP unit is brought to a complete stop within three seconds. The trip sequence and its implications on Well 1 are illustrated in figure 6.13.

The behavior of Well 1 during the trip sequence is similar to the behavior experienced during the shut-down sequence in section 6.4.2. This is not unexpected since the ESP unit is more or less operated in the same manner in both cases. The only difference in well operation in the respective cases is that the choke position is constant during the trip sequence while it is subject to changes during the shut-down sequence. Despite the fact that the choke is operated differently during the trip and shut-down sequence, the similar behavior is explained by taking the flow through the well into consideration. The main purpose of the wellhead choke is to control the flow through the well, and by examining figure 6.15 and 6.12 it is clear that there is little flow through the system when the ESP unit stopped. Since there is little flow through the system the behavior of the well is almost unaffected by the choke position.

Since the behavior of Well 1 during the trip sequence is similar to the behavior during the shut-down sequence, the influence on the manifold and the other wells in the system are also similar to the behavior observed in the shut-down sequence. This is evident by comparing figure 6.14 to figure 6.11, and figure 6.15 to figure 6.12. It should be noted that the frequency rate limitation during the trip sequence is a more extreme than the rate limitation during the shut-down sequence and this cause larger deflections. The arguments made with respect to figure 6.11 and 6.12 in section 6.4.2,

also applies to figure 6.14 and 6.15 and no further comments are added in this section.

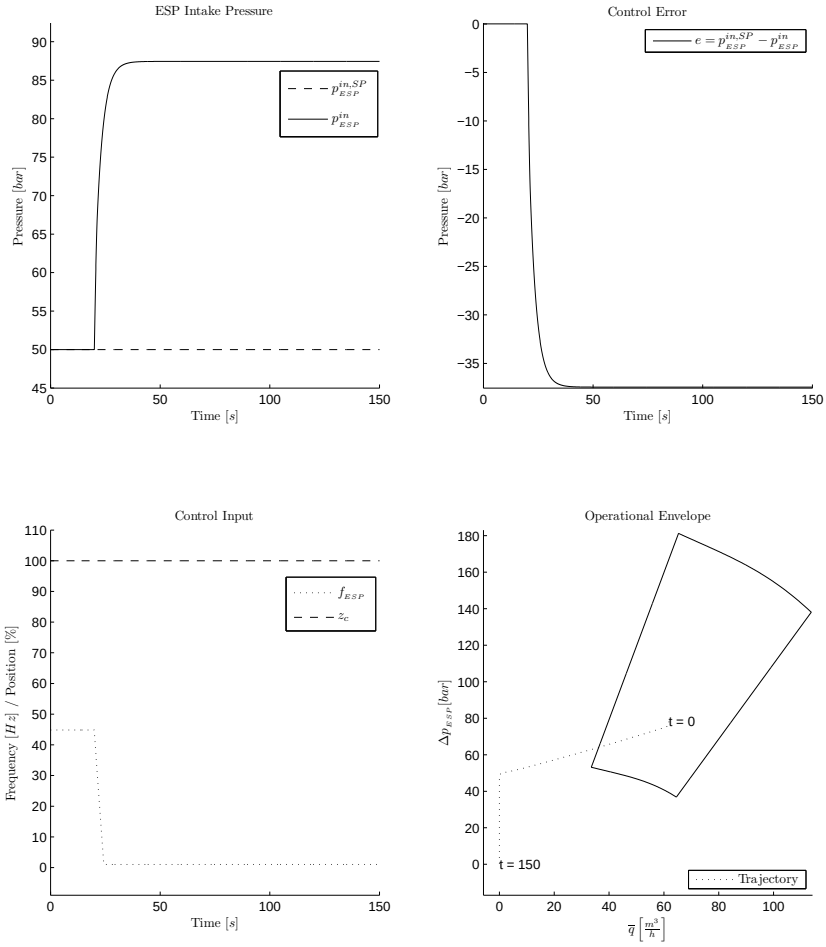

Figure 6.13: The trip sequence lead to a sudden drop in EPS frequency and consequently, a sudden stop in production from Well 1.

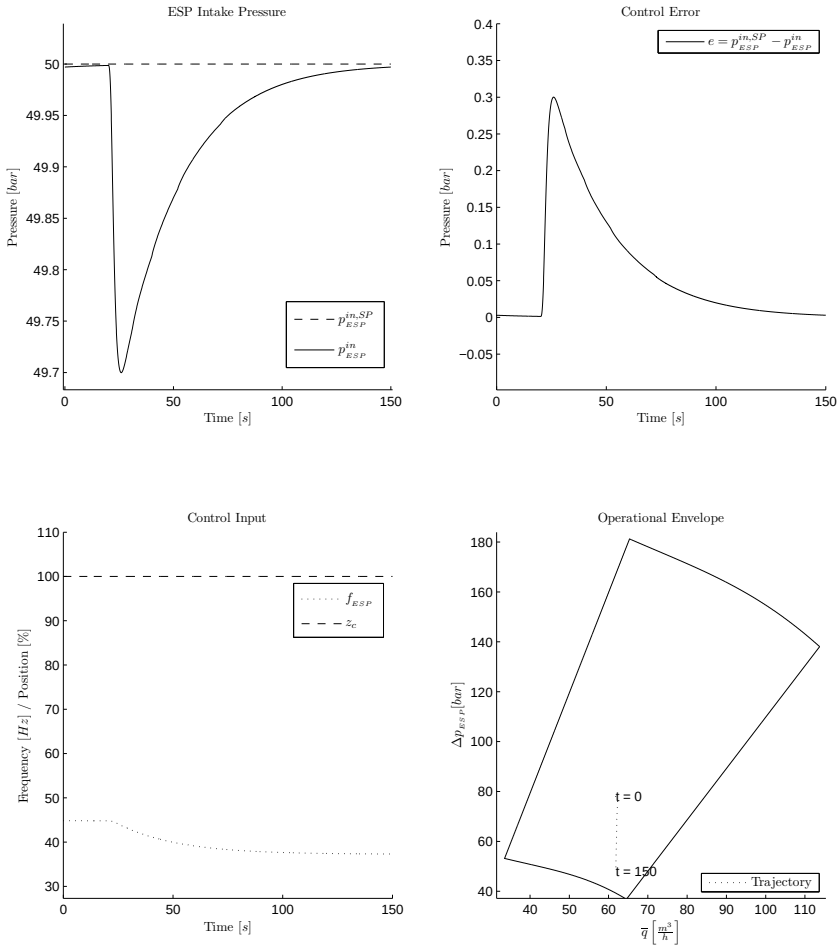

Figure 6.14: The trip sequence in Well 1 influence Well 2 and has the undesired effect of introducing a control error.

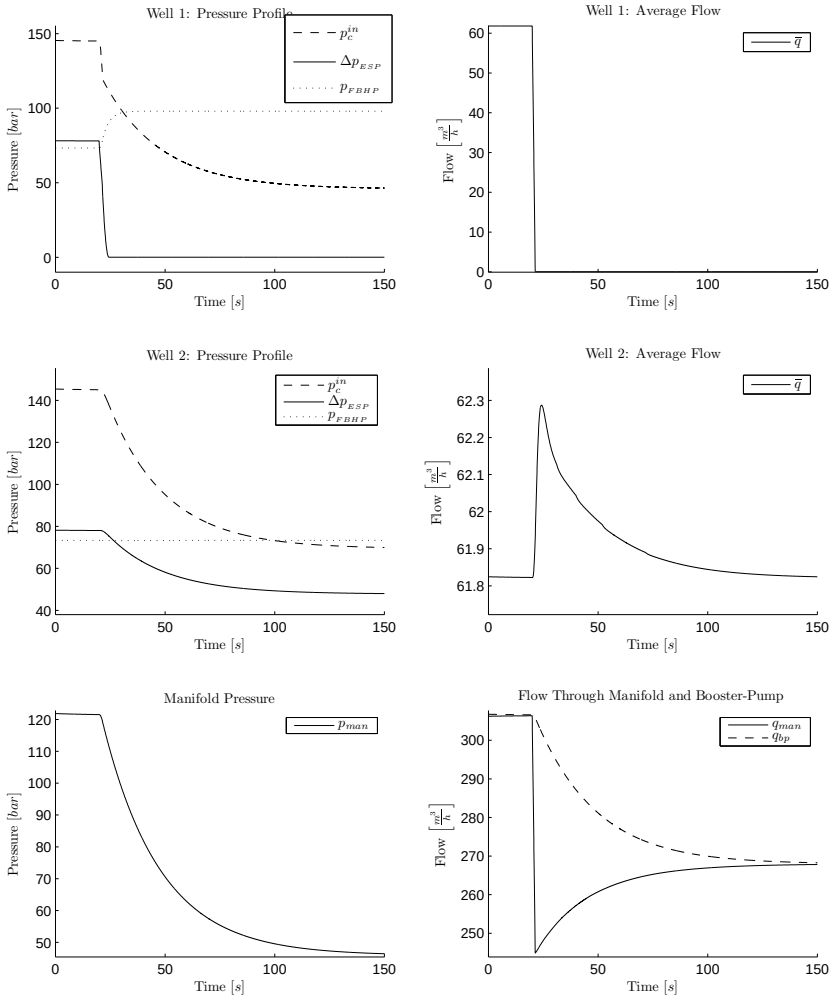

Figure 6.15: The trip sequence cause a sudden drop in pressure in Well 1 and, in turn, pressure drop in the manifold and in Well 2.

6.6 Scenario IV: Start-up/Shut-down of the booster-pump

The use of an additional pump, known as a booster-pump, located between the manifold and the transportation line is important for several reasons. The main purpose of the pump is to increase the pressure at the entry point of the transportation line to ensure that sufficient pressure is attained in order to overcome pressure loss along the flow path to the topside facility. In addition, as the following case study will show, the pump can also be used to support the control system in particular situations.

The booster-pump start-up scenario is presented in section 6.6.1, and the shut-down scenario is presented in section 6.6.2.

6.6.1 Case I: Starting up the booster-pump

This case study illustrate how a booster-pump start-up sequence influence the system and how active control of the booster-pump can be used to aid the pressure control system in situations where the control system is unable to attain the desired ESP intake pressure set-point.

Before the start-up sequence is initiated the pressure control system in Well 1 is unable to control the ESP intake pressure to the desired set-point, as seen from the control error trajectory in figure 6.16. At this point the ESP is operated at the maximum frequency and no "tiltak" can be employed to further reduce the control error.

The booster-pump start-up sequence is initiated after 20 seconds of simulation. During the start-up sequence the pump frequency is increased from 1Hz to 35Hz at a rate of 10Hz/s, and when the frequency reaches 35Hz it is further increased to 55Hz at a rate of 0.5Hz/s. The first stage of this start-up sequence coincides with the well start-up sequence. During the start-up sequence, the flow from the manifold through the transportation line gradually increases as the pressure at the entry point of the transportation line increase. At the same time, the manifold pressure decrease. This is seen from figure 6.18.

The decreasing pressure in the manifold cause a higher flow rate through the Well 1 and, in turn, this elevated flow rate enables the pressure control system to control the ESP intake pressure to the desired set-point. Thus, this case study shows how active operation of the booster-pump can be used to aid the pressure control system in the wells by managing the manifold pressure.

Well 2 is operated inside its operational envelope prior to the start-up

sequence and the pressure control system is able to attain the desired set-point. The varying manifold pressure during the start-up sequence has no positive effect on the operation of Well 2 and act only as a disturbance to the pressure control system. As seen from figure 6.17, the changes in manifold pressure cause a control error which initially was not present. In magnitude, the control error observed in this case is comparable to the one observed during ESP tripping.

Figure 6.18 contain little new and interesting information besides the points made in the previous sections.

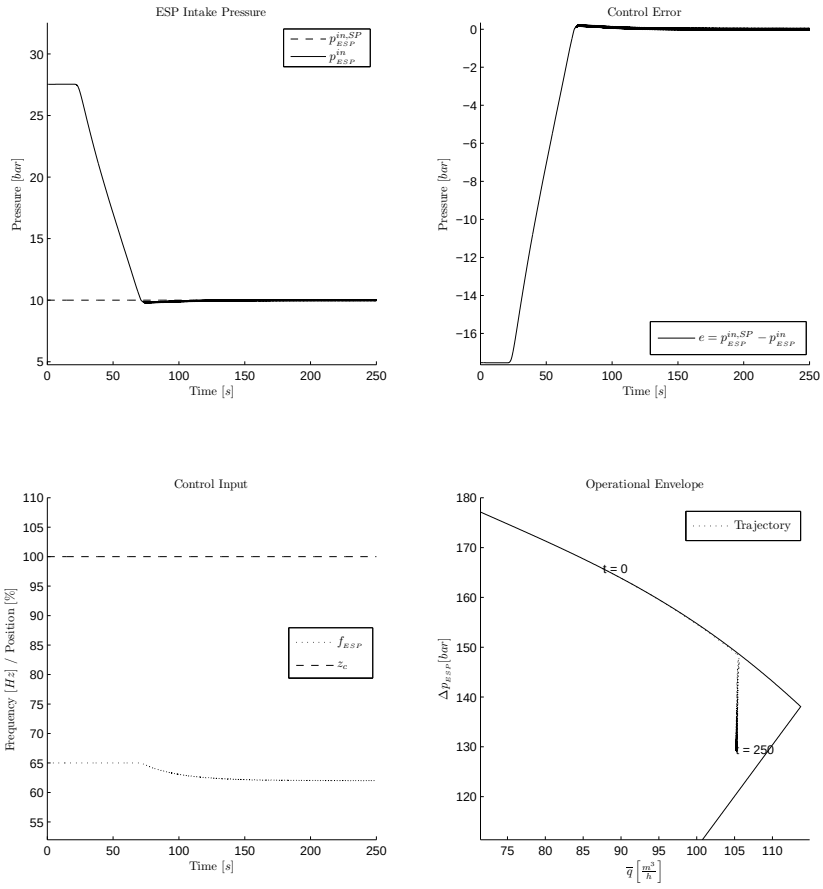

Figure 6.16: Starting up the booster-pump actively reduce the control error and thus, indirectly support the pressure control system in Well 1 by altering the manifold pressure.

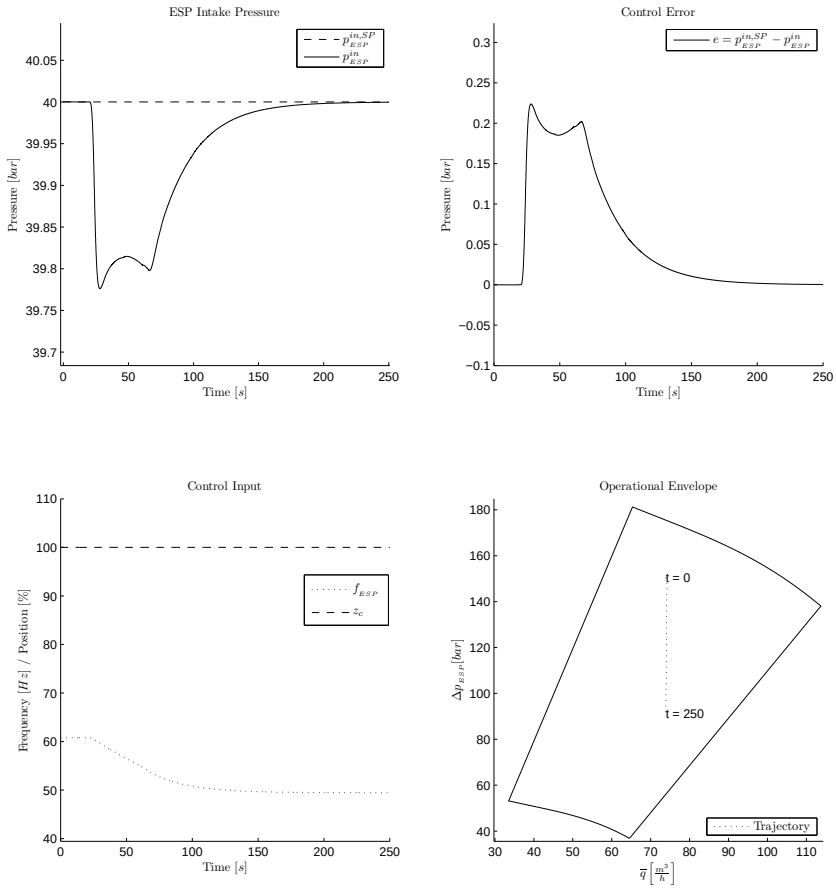

Figure 6.17: Booster pump start-up cause changes in manifold pressure which act as a disturbance to the control system in Well 2.

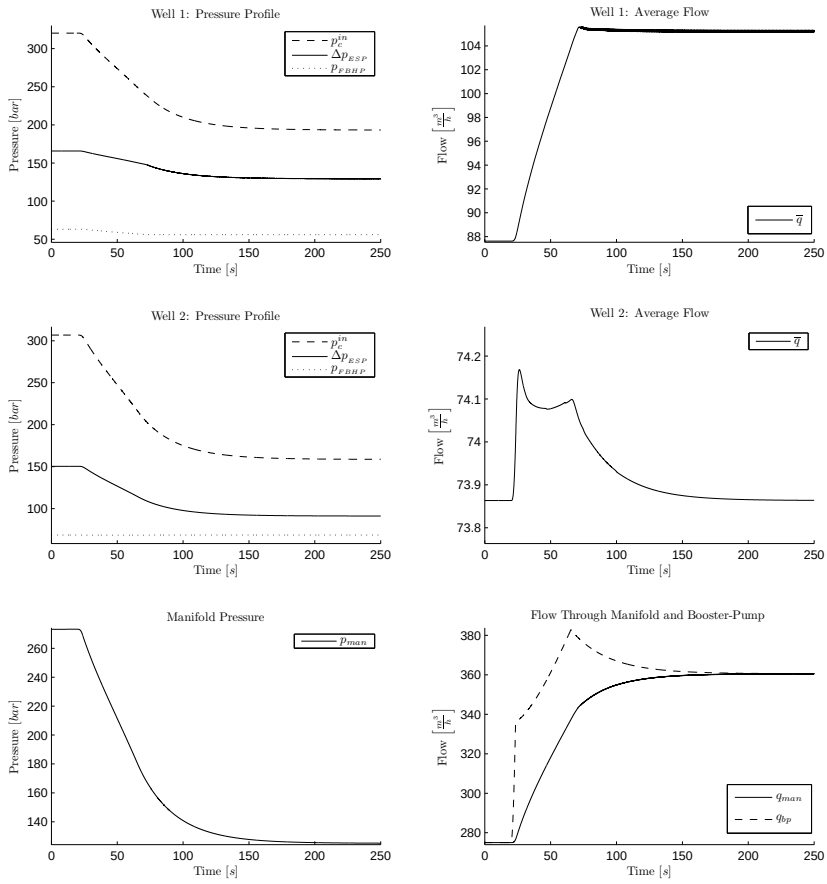

Figure 6.18: Influence on the pressure profiles and flow through both wells and the manifold.

6.6.2 Case II: Booster-pump shut-down

This case study show how two wells, running at different operating point, are influenced by a booster-pump shut-down. The shut-down sequence is initiated after 20 seconds of simulation and involves a gradual reduction in pump frequency down to 1Hz. The frequency rate limitation of 0.5Hz/s is upheld during the shut-down sequence.

In this situation the ESP intake pressure Well 1 is controlled to 30bar and the ESP unit is operated within the operational envelope. The ESP pressure in Well 2 is controlled to 50bar and, also, the ESP unit is operated with the operational envelope.

As the shut-down sequence is commenced the flow through from the manifold through the transportation line is gradually reduced and the pressure in the manifold increases. As figure 6.19 and 6.20 show, the changing manifold pressure act as a disturbance to the pressure control system in both wells and introduces a control error. Both control systems act by altering the ESP frequency to eliminate the control error. Even though the wells are operated about different ESP intake pressure set-points, they exhibit similar behavior during the booster-pump shut-down sequence.

Figure 6.21 supports the statements made in the previous paragraph. The pressure profile in Well 1 is similar to the pressure profile in Well 2, although the profiles are shifted pressure wise.

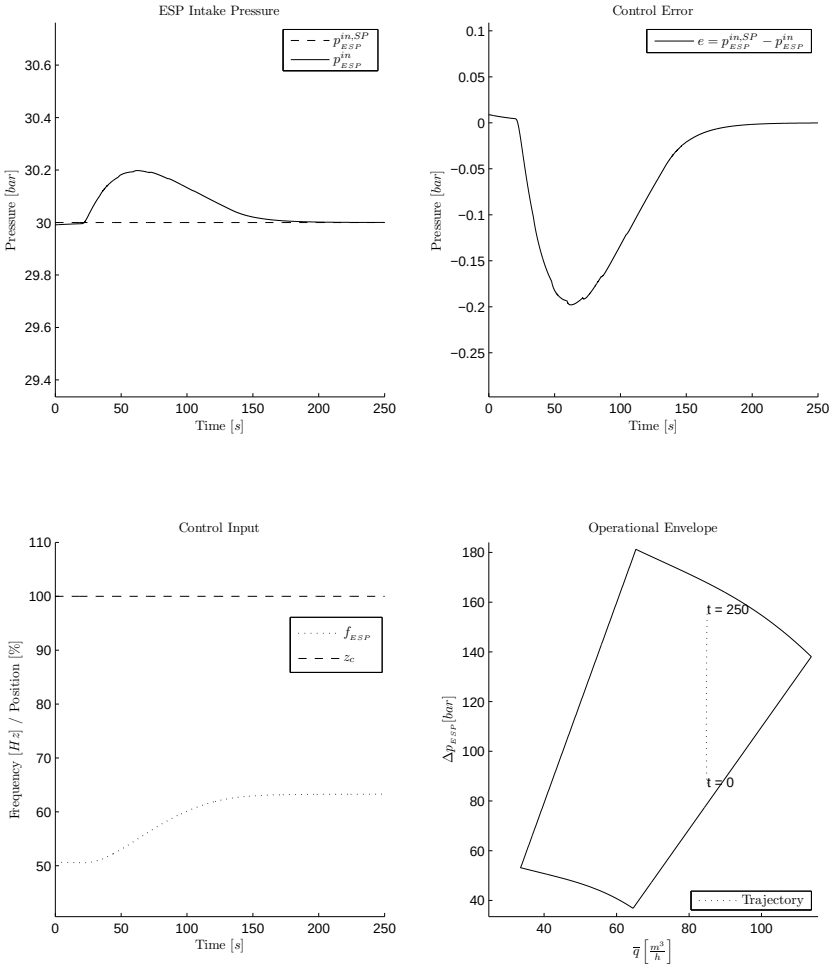

Figure 6.19: The booster-pump shut-down procedure put less strain on the control system than the start-up procedure.

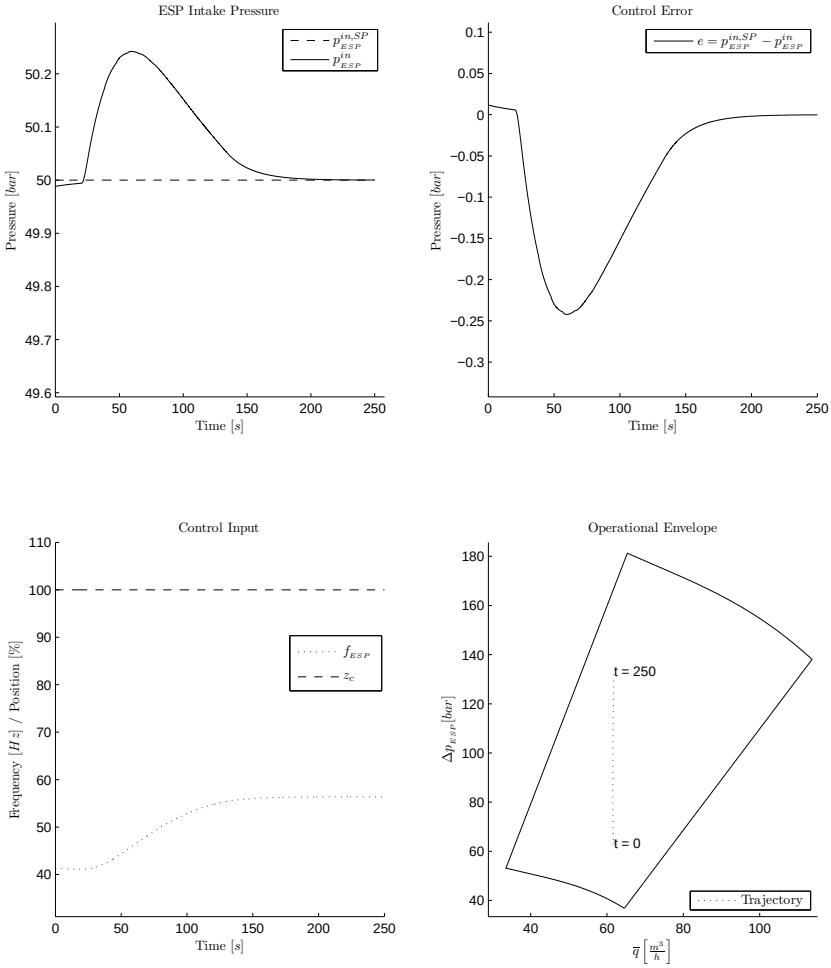

Figure 6.20: The same behavior is observed in both Well 1 and Well 2, even though the wells are operated about ESP pressure set-points.

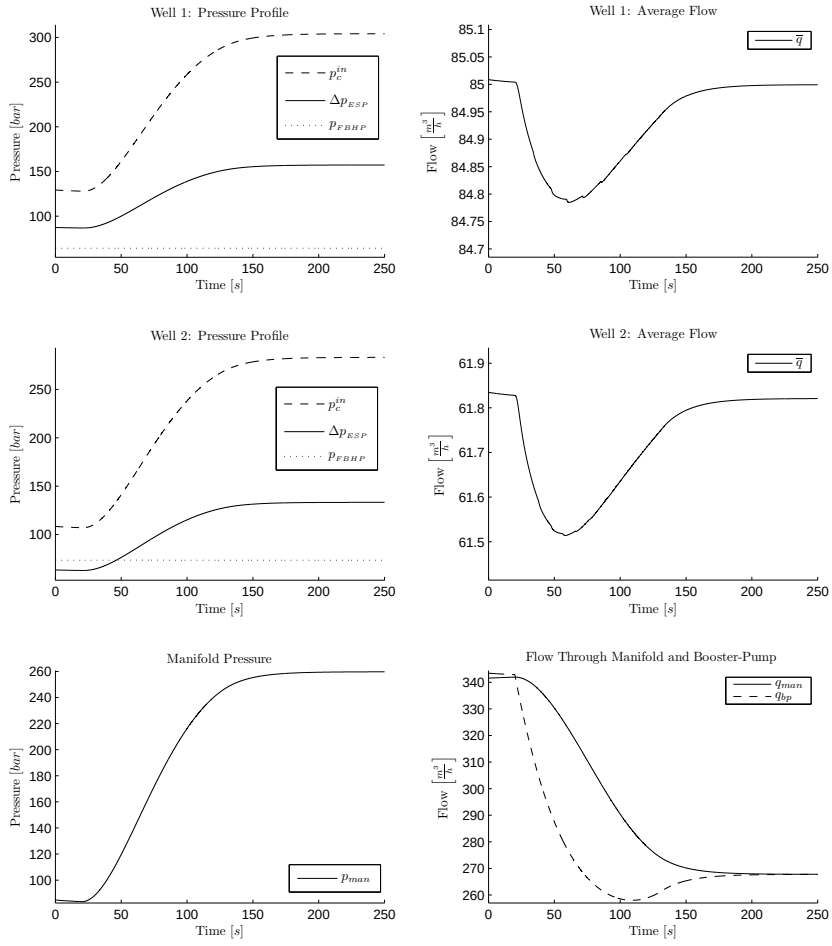

Figure 6.21: By shutting down the booster-pump the manifold pressure increase drastically and the flow from the manifold through the transportation line is reduced.

6.7 Concluding remarks

The simulation results indicate that there are some interactions between the wells in the system. The extent of interaction is influenced by the booster-pump operation, where a more prominent interaction is observed when the booster-pump is operated at low frequencies.

The control system display a capability of handling all the simulated situations by controlling the ESP intake pressure to the desired set-point while maintaining the ESP operated within the envelope. In those situations where it is not possible to reach the desired pressure set-point without violating the envelope, the control system converge to the operating point inside the envelope where the control error is minimum.

In those case study where a number of input combinations can be used to control the EPS intake pressure to the desired set-point, the control system converge to the combination of inputs where the choke position is as large as possible. A good illustration of this functionality is seen from figure 6.7 (the lowest, leftmost subfigure).

Chapter 7

Conclusion and future work

A mathematical model of a system containing four ESP lifted wells is created and implemented in MathWorks® MATLAB®. The model is an extension of the ESP model presented in Amundsen et al. [2010] and include four ESP lifted wells, a manifold, a booster-pump and a transportation line.

A pressure and envelope control system is proposed. The control system is designed based on a set control requirements related to handling of the operational envelope, ESP intake pressure control and input usage. The proposed control system fulfill the specified control requirements. The proposed control system is presented as an algorithm to simplify implementation of the system.

Open- and closed-loop stability properties of the mathematical model and the control system is investigated. Open-loop asymptotic stability is proven based on analysis of a linearized well model and the result is extended to the nonlinear model. Closed-loop stability is proven for the linearized well model based on frequency analysis. Closed-loop stability for the nonlinear well model is not proven, but a set of arguments are made that suggest that the system is passive and that passivity theory can be used to prove marginal stability of the system.

The mathematical model is simulated in closed-loop with the suggested control system. A set of different scenarios are simulated to investigate the behavior of system and to assess the control system capabilities of handling situations which is might to occur in a real life ESP lifted well system.

The simulation results show that the control system is able to handle the situations by keeping the ESP unit operated within the operational envelope.

7.1 Future work

The work presented in this report may be extended to other interesting control related topics. A short survey of relevant topics is presented here

- The proposed control system is not particulary well suited to handle situations where rapid changes occur in the system, this due to strict rate limitations on the control inputs. Better performance can be achieved if the control system is able to predict future behavior so that preventive action can be commenced.
- A relevant extention of the proposed control system is to control the ESP unit to its best efficiency point (BEP), where the ESP is utilized in the most cost effective manner.
- The composition of the product from all the wells may be controlled using a centralized control system on top of the proposed control system. In this way, the centralized controller can be used to derive optimal set-points the underlaying control systems.

Appendix A

Simulation environment

It is not within the scope of this thesis to provide a detailed description of the simulation environment. However, aspects that are considered to be particularly useful is described in this section.

A.1 System parameters

The model and control system is implemented using the following parameter values. Most of these values originate from the ESP model proposed by Amundsen et al. [2010].

Control volume 1 parameters

Parameter	Value	Unit	Description
β_1	$1.5 \cdot 10^9$	Pa	Compressibility
μ_1	0.3	$Pa \cdot s$	Viscosity
ρ_1	984	$\frac{kg}{m^3}$	Density
r_1	0.082	m	Radius
l_1	3078.8	m	Length
h_r	1029.2	m	Reservoar depth
h_p	920	m	ESP depth
B_0^1	$5.75 \cdot 10^6$		Friction constant
B_1^1	$3.90 \cdot 10^7$		Friction constant

Control volume 2 parameters

Parameter	Value	Unit	Description
β_2	$1.5 \cdot 10^9$	Pa	Compressibility
μ_2	4	$Pa \cdot s$	Viscosity
ρ_2	984	$\frac{kg}{m^3}$	Density
r_2	0.0595	m	Radius
l_2	922.2	m	Length
h_c	0	m	Choke depth
B_0^2	$7.45 \cdot 10^6$		Friction constant
B_1^2	$6.26 \cdot 10^7$		Friction constant

Controller parameters

Parameter	Value	Unit	Description
$\dot{f}_{ESP}^{MAX}$	0.5	$\frac{Hz}{s}$	Frequency rate limitation
$\dot{z}_c^{MAX}$	1/3	$\frac{\%}{s}$	Choke rate limitation
$\dot{f}_{BP}^{MAX}$	0.5	$\frac{Hz}{s}$	Frequency rate limitation
K_p	0.16		Proportional gain
τ_i	0.4		Integral time

Other parameters

Parameter	Value	Unit	Description
g	9.81	$\frac{m}{s^2}$	Gravitational acceleration
f_0	50	Hz	ESP base frequency
k	$1.12 \cdot 10^{-5}$	$\frac{m^3}{s \cdot Pa^{1/2}}$	Choke constant
PI	$6.9651 \cdot 10^{-9}$	$\frac{m^3}{Pa \cdot s}$	Productivity index
δt	0.05	s	Time step
WC	90	%	Water cut
$nStages$	64		Pump stages

A.2 Simulation and reproduction of results

The model is simulated by running the MATLAB-file `main.m` located in the folder `CD/Model/Run`.

The results from each case study in chapter 6 can be reproduced by commenting in the desired scenario/case in `main.m`:

```
%% Case select
% Case = 'ScenarioICaseI';
% Case = 'ScenarioICaseII';
% Case = 'ScenarioIICaseI';
% Case = 'ScenarioIICaseII';
% Case = 'ScenarioIIICaseI';
% Case = 'ScenarioIVCaseI';
% Case = 'ScenarioIVCaseII';
```

Appendix B

Mathematical deductions

B.1 Transfer function representation

The linearized system

$$\begin{aligned}\Delta\dot{\mathbf{x}} &= \begin{bmatrix} -a_{11} & 0 & -a_{13} \\ 0 & -a_{22} & a_{23} \\ a_{31} & -a_{32} & -a_{33} \end{bmatrix} \Delta\mathbf{x} + \begin{bmatrix} 0 & 0 \\ 0 & b_{22} \\ b_{31} & 0 \end{bmatrix} \Delta\mathbf{u} \\ &= \mathbf{A}\Delta\mathbf{x} + \mathbf{B}\Delta\mathbf{u}\end{aligned}$$

$$\begin{aligned}\Delta y &= \begin{bmatrix} 0 & 1 & c_{13} \end{bmatrix} \Delta\mathbf{x} + \begin{bmatrix} d_{12} & 0 \end{bmatrix} \overline{\mathbf{u}} \\ &= \mathbf{c}^\top\Delta\mathbf{x} + \mathbf{d}^\top\overline{\mathbf{u}}\end{aligned}$$

can be represented as a set of transfer functions using

$$\begin{aligned}\frac{\mathbf{Y}}{\mathbf{U}}(s) &= \mathbf{c}^\top \left(s\mathbf{I}_{3\times3} - \mathbf{A}\right)^{-1} \mathbf{B} \\ &= \mathbf{c}^\top \left|s\mathbf{I}_{3\times3} - \mathbf{A}\right|^{-1} adj\left(s\mathbf{I}_{3\times3} - \mathbf{A}\right) \mathbf{B} \\ &= \mathbf{G}(s)\end{aligned}$$

Neccesary derivations to obtain $\mathbf{G}(s)$ are performed in the following subsections.

Matrix invers

The invers of a matrix is given as the product of the invers determinant of the matrix and the adjoint of the matrix

$$(s\mathbf{I}_{3\times 3} - \mathbf{A})^{-1} = |s\mathbf{I}_{3\times 3} - \mathbf{A}|^{-1}\, adj\,(s\mathbf{I}_{3\times 3} - \mathbf{A})$$

The determinant and matrix adjoint are derived in the succeding sections.

Calculation of the determinant $|s\mathbf{I}_{3\times 3} - \mathbf{A}|$

The determinant polynomial, denoted $n(s)$, is calculated according to

$$\begin{aligned}
n(s) &= |s\mathbf{I}_{3\times 3} - \mathbf{A}| \\
&= \begin{vmatrix} s+a_{11} & 0 & a_{13} \\ 0 & s+a_{22} & -a_{23} \\ -a_{31} & a_{32} & s+a_{33} \end{vmatrix} \\
&= (s+a_{11})\left((s+a_{22})(s+a_{33}) - (-a_{23})\cdot a_{32}\right) + a_{13}\left(0\cdot a_{32} - (s+a_{22})(-a_{31})\right) \\
&= (s+a_{11})\left(s^2 + (a_{22}+a_{33})s + (a_{22}a_{33} + a_{23}a_{32})\right) + a_{13}a_{31}s + a_{13}a_{22}a_{31} \\
&= s^3 + (a_{11}+a_{22}+a_{33})\,s^2 + (a_{11}a_{22} + a_{11}a_{33} + a_{22}a_{33} + a_{23}a_{32} + a_{13}a_{31})\,s \\
&\qquad + (a_{11}a_{22}a_{33} + a_{11}a_{23}a_{32} + a_{13}a_{22}a_{31}) \\
&= n_3 s^3 + n_2 s^2 + n_1 s + n_0
\end{aligned}$$

Calculation of the adjoint matrix

The entries in the adjoint matrix M_{ij} is defined as the product of $(-1)^{i+j}$ and ij'th minor of $\mathbf{M}$. Thus, the adjoint matrix $\mathbf{M} = adj\,(s\mathbf{I}_{3\times 3} - \mathbf{A})$ is given according to

$$
\begin{aligned}
\mathbf{M} &= adj\,(s\mathbf{I}_{3\times 3} - \mathbf{A}) \\
&= \begin{bmatrix}
\begin{vmatrix} s+a_{22} & -a_{23} \\ a_{32} & s+a_{33} \end{vmatrix} & -\begin{vmatrix} 0 & -a_{23} \\ -a_{31} & s+a_{33} \end{vmatrix} & \begin{vmatrix} 0 & s+a_{22} \\ -a_{31} & a_{32} \end{vmatrix} \\
-\begin{vmatrix} 0 & a_{13} \\ a_{32} & s+a_{33} \end{vmatrix} & \begin{vmatrix} s+a_{11} & a_{13} \\ -a_{31} & s+a_{33} \end{vmatrix} & -\begin{vmatrix} s+a_{11} & 0 \\ -a_{31} & a_{32} \end{vmatrix} \\
\begin{vmatrix} 0 & a_{13} \\ s+a_{22} & -a_{23} \end{vmatrix} & -\begin{vmatrix} s+a_{11} & a_{13} \\ 0 & -a_{23} \end{vmatrix} & \begin{vmatrix} s+a_{11} & 0 \\ 0 & s+a_{22} \end{vmatrix}
\end{bmatrix} \\
&= \begin{bmatrix}
(s+a_{22})(s+a_{33}) + a_{23}a_{32} & a_{23}a_{31} & (s+a_{22})\,a_{31} \\
a_{13}a_{32} & (s+a_{11})(s+a_{33}) + a_{13}a_{31} & -(s+a_{11})\,a_{32} \\
-a_{13}(s+a_{22}) & (s+a_{11})\,a_{23} & (s+a_{11})(s+a_{22})
\end{bmatrix} \\
&= \begin{bmatrix}
s^2 + (a_{22}+a_{33})\,s + (a_{22}a_{33} + a_{23}a_{32}) & a_{23}a_{31} & a_{31}s + a_{22}a_{31} \\
a_{13}a_{32} & s^2 + (a_{11}+a_{33})\,s + a_{11}a_{33} + a_{13}a_{31} & -a_{32}s - a_{11}a_{32} \\
-a_{13}s - a_{13}a_{22} & a_{23}s + a_{11}a_{23} & s^2 + (a_{11}+a_{22})\,s + a_{11}a_{22}
\end{bmatrix} \\
&= \begin{bmatrix}
M_{11}(s) & M_{12} & M_{13}(s) \\
M_{21} & M_{22}(s) & M_{23}(s) \\
M_{31}(s) & M_{32}(s) & M_{33}(s)
\end{bmatrix}
\end{aligned}
$$

Derivation of $H(s)$

Based on the derived expression of the determinant and adjoint matrix in the previous sections, the following expression for the transfer functions are obtained

$$\begin{aligned}
\mathbf{G}(s) &= \mathbf{c}^\top |s\mathbf{I}_{3\times 3} - \mathbf{A}|^{-1} adj\,(s\mathbf{I}_{3\times 3} - \mathbf{A})\,\mathbf{B} + \mathbf{d}^\top \\
&= \begin{bmatrix} 1 & 0 & -c_{13} \end{bmatrix} \frac{1}{n(s)} \begin{bmatrix} M_{11}(s) & M_{12} & M_{13}(s) \\ M_{21} & M_{22}(s) & M_{23}(s) \\ M_{31}(s) & M_{32}(s) & M_{33}(s) \end{bmatrix} \begin{bmatrix} 0 & 0 \\ 0 & b_{22} \\ b_{31} & 0 \end{bmatrix} + \begin{bmatrix} d_{12} & 0 \end{bmatrix} \\
&= \frac{1}{n(s)} \begin{bmatrix} 1 & 0 & -c_{13} \end{bmatrix} \begin{bmatrix} b_{31}M_{13}(s) & b_{22}M_{12} \\ b_{31}M_{23}(s) & b_{22}M_{22}(s) \\ b_{31}M_{33}(s) & b_{22}M_{32}(s) \end{bmatrix} + \begin{bmatrix} d_{12} & 0 \end{bmatrix} \\
&= \frac{1}{n(s)} \begin{bmatrix} b_{31}M_{13}(s) - c_{13}b_{31}M_{33}(s) & b_{22}M_{12} - c_{13}b_{22}M_{32}(s) \end{bmatrix} + \begin{bmatrix} d_{12} & 0 \end{bmatrix} \\
&= \begin{bmatrix} \frac{b_{31}M_{13}(s) - c_{13}b_{31}M_{33}(s) + d_{12}n(s)}{n(s)} & \frac{b_{22}M_{12} - c_{13}b_{22}M_{32}(s)}{n(s)} \end{bmatrix}
\end{aligned}$$

Inserting for $M_{13}(s)$, $M_{33}(s)$, M_{12}, $M_{32}(s)$ and $d(s)$ yield

$$\begin{aligned}
\mathbf{G}(s) &= \begin{bmatrix} \frac{b_{31}(a_{31}s + a_{22}a_{31}) - c_{13}b_{31}\left(s^2 + (a_{11}+a_{22})s + a_{11}a_{22}\right) + d_{12}\left(n_3s^3 + n_2s^2 + n_1s + n_0\right)}{n_3s^3 + n_2s^2 + n_1s + n_0} \\ \qquad\qquad \frac{b_{22}(a_{23}a_{31}) - c_{13}b_{22}(a_{23}s + a_{11}a_{23})}{n_3s^3 + n_2s^2 + n_1s + n_0} \end{bmatrix} \\
&= \begin{bmatrix} \frac{d_{12}n_3s^3 + (d_{12}n_2 - b_{31}c_{13})s^2 + (d_{12}n_1 + b_{31}(a_{31} - (a_{11}+a_{22})c_{13}))s + d_{12}n_0 + a_{22}b_{31}(a_{31} - a_{11}c_{13})}{n_3s^3 + n_2s^2 + n_1s + n_0} \\ \qquad\qquad \frac{b_{22}(a_{23}a_{31}) - c_{13}b_{22}(a_{23}s + a_{11}a_{23})}{n_3s^3 + n_2s^2 + n_1s + n_0} \end{bmatrix} \\
&= \begin{bmatrix} G_1(s) & G_2(s) \end{bmatrix} \qquad \text{(B.1)}
\end{aligned}$$

B.2 Nonlinear control law

A set of nonlinear control laws that ensure closed-loop exponential stability can be derived using Lyapunov theory, starting with the positive definite Lyapunov function candidate

$$V(x_1, x_2, x_3) = \frac{1}{2}\frac{V_1}{\beta_1}x_1^2 + \frac{1}{2}\frac{V_2}{\beta_2}x_2^2 + \frac{1}{2}\frac{\overline{\rho}\overline{l}}{\overline{A}}x_3^2$$

The derivative of $V(x_1, x_2, x_3)$ in the direction of the system (5.1) is given by

$$\begin{aligned}\dot{V} = \frac{\delta V}{\delta x} &= \sum_{i=1}^{3}\frac{\delta V}{\delta x_i}\dot{x}_i = \sum_{i=1}^{3}\frac{\delta V}{\delta x_i}f_i \\ &= \begin{bmatrix} \frac{\delta V}{\delta x_1} & \frac{\delta V}{\delta x_2} & \frac{\delta V}{\delta x_3} \end{bmatrix}\begin{bmatrix} f_1(\mathbf{x}) \\ f_2(\mathbf{x},\mathbf{u}) \\ f_3(\mathbf{x},\mathbf{u}) \end{bmatrix}\end{aligned}$$

Inserting the partial derivatives of $V(x_1, x_2, x_3)$ yield

$$\begin{aligned}\dot{V} &= \begin{bmatrix} \frac{V_1}{\beta_1}x_1 & \frac{V_2}{\beta_2}x_2 & \frac{\overline{\rho}\overline{l}}{\overline{A}}x_3 \end{bmatrix} \\ &\quad \cdot \begin{bmatrix} \frac{\beta_1}{V_1}\left(PI\left(p_r - x_1\right) - x_3\right) \\ \frac{\beta_2}{V_2}\left(x_3 - k\sqrt{x_2 - p_{man}}u_2\right) \\ \frac{\overline{A}}{\overline{\rho}\overline{l}}\Big(x_1 - x_2 + \rho_1 g\frac{H_0}{f_0^2}u_1^2(u_1,u_2) - \frac{\left(B_0^1+B_1^1\right)}{A_1}\frac{\rho_1}{2}x_3^2 - \frac{\left(B_0^2+B_1^2\right)}{A_2}\frac{\rho_2}{2}x_3^2 \\ \qquad -\rho_1 g(h_r - h_p) - \rho_2 g(h_p - h_c)\Big) \end{bmatrix} \\ &= PIp_r x_1 - PIx_1^2 - \cancel{x_1x_3} + \cancel{x_2x_3} - k\sqrt{x_2 - p_{man}}x_2u_2 + \cancel{x_1x_3} - \cancel{x_2x_3} \\ &\quad + \rho_1 g\frac{H_0}{f_0^2}u_1^2x_3 - \frac{\left(B_0^1+B_1^1\right)}{A_1}\frac{\rho_1}{2}x_3^3 - \frac{\left(B_0^2+B_1^2\right)}{A_2}\frac{\rho_2}{2}x_3^3 \\ &\quad - \rho_1 g(h_r - h_p)x_3 - \rho_2 g(h_p - h_c)x_3 \\ &= -PIx_1^2 - x_2^2 - x_3^2 + \phi(\mathbf{x},\mathbf{u})\end{aligned}$$

where

$$\begin{aligned}\phi(\mathbf{x},\mathbf{u}) &= PIp_r x_1 - k\sqrt{x_2 - p_{man}}x_2 u_2 + \rho_1 g\frac{H_0}{f_0^2}u_1^2 x_3 - \frac{\left(B_0^1 + B_1^1\right)}{A_1}\frac{\rho_1}{2}x_3^3 \\ &\quad -\frac{\left(B_0^2 + B_1^2\right)}{A_2}\frac{\rho_2}{2}x_3^3 - \rho_1 g(h_r - h_p)x_3 - \rho_2 g(h_p - h_c)x_3 + x_2^2 + x_3^2\end{aligned}$$

By selecting any combination of u_1 and u_2 that satisfy $\phi(\mathbf{x},\mathbf{u}) = 0$, $\dot{V}$ become

$$\dot{V} = -PIx_1^2 - x_2^2 - x_3^2$$

and the closed-loop system satisfy the requirements of being exponentially stable according to Khalil [2002, Theorem 4.10].

Appendix C

CD contents

This report includes a CD that contains this report in a portable document format (PDF), referenced articles and MATLAB code.

The content is organized as follows

- Report.pdf - File
- Bibliography - Folder
- MATLABcode - Folder

Bibliography

This folder contain referenced articles in the Bibliography. The following articles are included

- *Automatic start up of ESP-lifted wells* by Amundsen, Zhou and Scherrer.
- *Stabilization of Gas Distribution Instability in Single Point Dual Gas-LiftWells* by Eikrem, Aamo and Foss.
- *A new friction factor relationship for fully developed pipe flow* by McKeon, Zagarola and Smits.

MATLABcode

This folder contains the m-files, organized into subfolders as follows.

- The folder *run* contains the following m-files:

Path	***Filename***
run	*main.m*
run>Data	*parameters.m*
	createDataVectors.m
	draw.m
	saveData.m
	simulation.m

- The folder *Generic* contains the following m-files:

Path	***Filename***
Generic>Analysis	*linearizedModel.m*
Generic>Control	*ControlAlgorithm.m*
	DynamicSaturationLimits.m
	UpdateF_ESP.m
	UpdateZ_c.m
	WaterFeedControl.m
Generic>Examples>Example31	*Example31.m*
Generic>ManifoldModules	*CreateManifold.m*
	dpBP.m
	SimManifold.m
	SolveDiffEqManifold.m
	TLFriction.m
	UpdateManifold.m
Generic>Other	*CalculateBounds.m*
	dpESPBounds.m
Generic>Statoil	*choke.m*
	ChokeCharacteristics.m
	dpESP
	Friction.m
	ode4.m
Generic>WellModules	*CreateWell.m*
	DiffEquations.m
	FlowProfile.m
	PressureProfile.m
	SimWell.m
	SingleWellInit.m
	SolveDiffEqWell.m
	UpdateProfileWell.m

- The folder *Scenario* contains the following m-files:

Path	***Filename***
Scenario	*ScenarioICase01.m*
	ScenarioICase02.m
	ScenarioIICase01.m
	ScenarioIICase02.m
	ScenarioIIICase01.m
	ScenarioIVCase01.m
	ScenarioIVCase02.m
Scenario>Subfunctions	*ESPtripping.m*
	ShutDown.m
	StartUp.m

Bibliography

D. Amundsen, W. Zhou, and A. Scherrer. Automatic start up of ESP-lifted wells. Summer project in association with Statoil ASA, 2010.

J. G. Balchen, T. Andresen, and B. A. Foss. *Reguleringsteknikk.* Tapir Trykkeri, Trondheim, 2004.

Chi-Tsong Chen. *Linear System Theory and Design.* Oxford University Press, Inc., 1999.

O. Egeland and J. T. Gravdahl. *Modeling and Simulation for Automatic Control.* Tapir Trykkeri, Trondheim, 2003.

G. O. Eikrem, O. M. Aamo, and B. A. Foss. Stabilization of Gas Distribution Instability in Single Point Dual Gas-Lift Wells. *Society of Petroleum Engineers (SPE)*, 21:252–259, 2006.

H. K. Khalil. *Nonlinear Ssystems.* Prentice Hall, Inc., 2002.

B. J. McKeon, M. V. Zagarola, and A. J. Smits. A new friction factor relationship for fully developed pipe flow. *The Journal of Fluid Mechanics*, 538:429–443, 2005.

S. Skogestad and I. Postlethwaite. *Multivariabl eFeedback Control.* John Wiley & Sons Ltd., The Atrium, Southern Gate, Chichester, 2005.

G. Takacs. *Electrical Submersible Pumps Manual.* Gulf Professional Publishing, Elsevier, 2009.

F. M. White. *Fluid Mechanics.* McGraw-Hill Companies, 2008.